UNIVERSITY OF TURKU

# Selection of a Polymer Additive Manufacturing Method for a Medical Device Prototype

A two-component decision-making model

Faculty of Technology
Department of Mechanical and Materials Engineering
Mechanical Engineering in Digital Design
Master's thesis (in Technology)

Author:
Tatu Hanski

26.5.2026
Turku

Master's thesis (in Technology)

**Subject**: Decision-making in selecting an additive manufacturing method for a medical device prototype context
**Author**: Tatu Hanski
**Title**: Selection of a polymer additive manufacturing method for a medical device prototype
**Supervisor(s)**: Docent Heidi Piili, M.Sc. (Tech) Iiro Mäkinen
**Number of pages**: 84 pages
**Date**: 26.5.2026

Polymer additive manufacturing (AM) offers design flexibility, patient specific geometries and reduced expensive waste material, making AM an interesting choice for fabricating small and complex medical devices. The selection of a suitable polymer AM method is however not straightforward, as no single AM method is optimal for all criteria for medical devices. The aim of this thesis was to determine the most suitable polymer AM method for fabricating small biodegradable stent-like medical device prototypes, and to provide a transparent, repeatable decision-making framework which supports the selection process in different prototyping contexts.

Literature review of this thesis studies the use of polymer AM in biomedical applications, with a focus on bioresorbable vascular stents. The five main polymer AM methods were reviewed: material extrusion, vat photopolymerization, material jetting, binder jetting and powder bed fusion. The methods were compared to each other against nine comparison criteria covering manufacturing accuracy, biocompatible and biodegradable material availability, and post-processing requirements. Main findings of the literature review realized material regulatory and biocompatibility as hard constraints for intravascular implant use, and resolution limitations and surface roughness as challenges in manufacturing stent-like devices.

The experimental part of this thesis built a two-component decision-making framework. A decision-making tree filters non-suitable polymer AM methods based on hard constraints depending on the use case of the prototype. Analytical hierarchy process (AHP) method compares the importance of the nine comparison criteria, based on which the different polymer AM methods were compared. AHP produces context-dependent weight factors for different prototyping scenarios, depending on the order of importance of the comparison criteria. The logical coherence of the weight factors are verified through consistency ratio calculations. The model was tested with two prototyping scenarios: implantable or *in vivo* prototypes (scenario 1) and geometry-only functional prototypes (scenario 2). For scenario 1, powder bed fusion was the best method by a wide margin. Material jetting, vat photopolymerization and powder bed fusion were first, second and third respectively for scenario 2, but with a fine margin. Consistency ratio calculations confirmed logical coherence for both scenario weight factors.

The decision-making framework produced logical and consistent results and provided fitting rankings for the five polymer AM methods for each scenario. This demonstrated that the choice of a suitable AM method for producing medical device prototypes can be transparently determined through combining hard constraints of the decision-making tree and the AHP method for multi-criteria comparison of different AM methods. Model improvement suggestions include adding automatization for the weight factor calculations to reduce laboriousness of the AHP process with nine comparison criteria, and to include expert views from multiple disciplines of a medical device development team to make the results more objective.

**Key words**: Polymer additive manufacturing, prototyping, medical device, decision-making tree, analytical hierarchy process.

Muovien lisäävä valmistus (engl. additive manufacturing, AM) mahdollistaa joustoa tuotesuunnittelussa, potilaskohtaisia geometrioita ja kalliin hukkamateriaalin vähentämistä. Tämä tekee lisäävän valmistuksen menetelmistä kiinnostavia vaihtoehtoja pienten ja monimutkaisten lääkinnällisten laitteiden valmistusmenetelmäksi. Lisäävän valmistusmenetelmän valinta ei kuitenkaan ole suoraviivaista, koska yksikään menetelmistä ei ole edullinen kaikkien lääkinnällisen laitteen vaatimuksien täyttämiselle. Tämän opinnäytetyön tarkoitus oli määrittää parhaiten soveltuva muovien lisäävä valmistusmenetelmä pienten biohajoavien stenttimäisten lääkinnällisten laitteiden prototyyppivalmistukselle ja antaa läpinäkyvä ja toistettava päätöksentekomalli, joka tukee menetelmävalintaa erilaisissa prototyyppauskonteksteissa.

Lisäävän valmistuksen käytöstä biolääkinnällisessä sektorissa tehtiin kirjallisuuskatsaus, jossa painotettiin erityisesti biohajoavien vaskulaaristenttien valmistusta eri menetelmillä. Työssä käsiteltiin viisi muovien lisäävän valmistuksen menetelmää: materiaalin pursotus (engl. material extrusion, MEX), valokovetus altaassa (engl. vat photopolymerization, VPP), materiaalin suihkutus (engl. material jetting, MJT), sideaineen suihkutus (engl. binder jetting, BJT) ja jauhepetisulatus (engl. powder bed fusion, PBF). Menetelmiä verrattiin toisiinsa yhdeksän vertailukriteerin avulla. Vertailukriteerit kattoivat valmistustarkkuuden, materiaalivalikoiman bioyhteensopivuuden ja biohajoavuuden ja jälkikäsittelytarpeet. Kirjallisuuskatsauksen päälöytöjä olivat materiaalien regulaatio- ja bioyhteensopivuusvaatimusten asettamat jyrkät rajat suonensisäisen implantin valmistuksessa, sekä valmistustarkkuuden ja pinnankarkeuden aiheuttamat haasteet stenttimäisten laitteiden valmistuksessa.

Kokeellisessa osiossa rakennettiin kaksiosainen päätöksentekomalli. Päätöksentekopuu karsi epäsopivat menetelmät riippuen prototyypin käyttötarkoituksen asettamista vaatimuksista. Analyyttistä hierarkiaprosessia (engl. analytical hierarchy process, AHP) käytettiin lisäävien valmistusmenetelmien vertailukriteerien priorisoinnissa eri prototyyppikonteksteille. AHP-menetelmä tuotti kontekstiriippuvaiset painokertoimet vertailukriteereille, minkä pohjalta lisäävät valmistusmenetelmät pisteytettiin. Painokertoimien looginen johdonmukaisuus varmennettiin konsistenssisuhdelaskelmilla. Päätöksentekomallia testattiin kahdella prototyyppiskenaariolla. Skenaario 1 käsitteli implantoitavaa tai elävän kudoksen kanssa kosketuksissa olevaa prototyyppiä, ja skenaario 2 käsitteli toiminnallista geometriamallia, joka ei ole elävän kudoksen kanssa kosketuksessa. Jauhepetisulatus oli selvästi paras valinta skenaariolle 1, ja skenaariolle 2 materiaalin suihkutus, valopetikovetus ja jauhepetisulatus olivat sijoilla 1., 2. ja 3. Erot skenaariolle 2 olivat kuitenkin hyvin pieniä. Konsistenssisuhdelaskelmat varmensivat molempien skenaarioiden painokertoimien loogisen johdonmukaisuuden.

Päätöksentekomalli tuotti loogisia ja johdonmukaisia tuloksia ja asetti eri valmistusmenetelmät sopivaan järjestykseen molemmille skenaarioille. Tulokset osoittivat, että lisäävän valmistuksen menetelmän valinta voidaan tehdä läpinäkyvällä tavalla yhdistämällä päätöksentekopuun jyrkät vaatimukset karsimaan epäsopivat menetelmät pois ja AHP-menetelmän monikriteerisen vertailun eri valmistusmenetelmien välillä. Mallin parannusehdotuksia olivat muun muassa automatisaation lisääminen työlään yhdeksän kriteerin vertailuvaiheen nopeuttamiseksi, sekä tuotekehitystiimin eri alan asiantuntijoiden syötteet vertailukriteerien paremmuusjärjestykseen asettamiseksi, jotta painokertoimet olisivat objektiivisempia.

**Avainsanat**: Muovien lisäävä valmistus, prototyyppaus, lääkinnällinen laite, päätöksentekopuu, analyyttinen hierarkiaprosessi.

# Table of contents

## Nomenclature

| Symbol | Explanation |
|---|---|
| $\lambda_{max}$ | Largest eigenvalue, mean of $d_i$ / $w_i$ values |
| CI | Consistency index |
| CR | Consistency ratio |
| $d_i$ | Weighted sum vector |
| n | Dimension of the pairwise comparison matrix |
| RI | Random index |
| $w_i$ | Weight factor for criterion i derived from AHP method |

| Abbreviation | Explanation |
|---|---|
| 3D | Three-dimensional |
| AHP | Analytical hierarchy process |
| AM | Additive manufacturing |
| AMed | Additively manufactured |
| BCP | Biphasic calcium phosphate |
| BJT | Binder jetting |
| BRS | Bioresorbable stent |
| CAD | Computer aided design |
| CLIP | Continuous liquid interface production |
| CO2 | Carbon dioxide |
| CVDs | Cardiovascular diseases |
| DLP | Digital light processing |
| DMD | Digital micromirror device |
| EC | European Commission |
| FDA | U.S. Food and drug administration |
| G-code | Machine code for AM machinery |
| LCD | Liquid crystal display |
| MEX | Material extrusion |
| MJT | Material jetting |
| PA | Polyamide |
| PBF | Powder bed fusion |
| PBF-EB | Powder bed fusion with electron beam melting |
| PBF-LB | Powder bed fusion with laser beam melting |
| PBF-LB/P | Powder bed fusion with electron beam melting of polymers |
| PCL | Polycaprolactone |
| PLA | Polylactic acid |
| PLGA | Poly(lactic-co-glycolic) acid |
| PLLA | poly l-lactic acid |
| SLA | Stereolithography |
| STL | Standard Tesselation Language |
| TPP | two-photon polymerization |
| UV | ultraviolet |
| VPP | Vat photopolymerization |

# 1 Introduction

According to ISO 52900 standard, additive manufacturing (AM) is a process of successively joining material layer-by-layer to produce an object based on three-dimensional (3D) digital model. In other words, AM, also called industrial 3D printing, manufactures products by selectively adding material, whereas conventional subtractive methods remove material to create desired shapes, and formative methods apply pressure to the raw material to change the shape of the part (Chartrain et al., 2018). Conventional methods use for example machining and casting to create products (Khalaj et al., 2021). Advantages for AM comparing to conventional methods are for example reduced amount of waste materials in production, flexibility in geometric design of the manufactured products, customizability, and possibility of localized production where the parts made with AM are used in applications (Zhu et al., 2025). A typical state-of-the-art procedure for an AM process is shown in Figure 1.

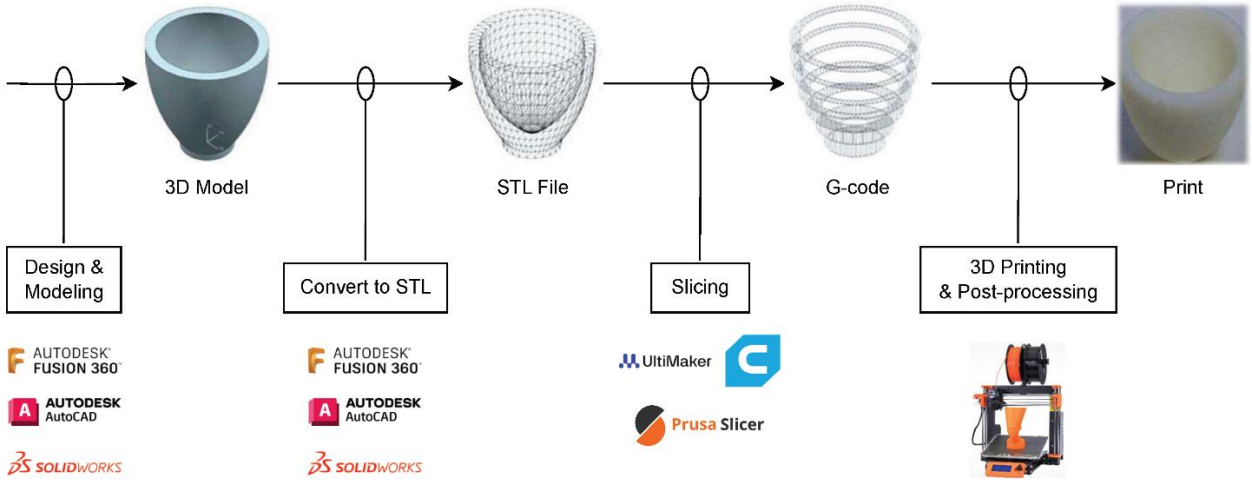


**Figure 1. Common AM process workflow.** From left to right the AM process starts from design of the product with a CAD software, converting the 3D model into STL-format, slicing the STL-file with a dedicated slicer software, which creates the G-code the AM machine uses for the manufacturing process. Figure from Zhou et al. (2024).

As shown in Figure 1, a common AM process begins by importing a computer aided design (CAD) file, which includes data about the 3D geometry of the component, to a standardized format, such as a standard tessellation language (STL). The standardized file is then imported to a slicer software. The slicer software sets the manufacturing parameters, such as layer thickness, material choice, infill density, and manufacturing speed of the AM process. The model is sliced to equally thin layers, and the machine code (G-code) is created for the AM machine. G-code contains the information on where the material is selectively added or

solidified on the build platform. (Dobrzańska-Danikiewicz & Bączyk, 2024; Zhou et al., 2024) Figure 1 does not include the post-processing steps for an additively manufactured (AMed) part. Post processing may include removal of support structures and other thermal, chemical or mechanical surface treatments.

Different AM methods are classified by the kinds of raw materials used, and what energy application method is used to selectively join the material (Ali et al., 2024; *ISO/ASTM 52900:2021(En), Additive Manufacturing — General Principles — Fundamentals and Vocabulary*). For example, vat photopolymerization (VPP) methods solidify liquid photosensitive resins with a laser beam or ultraviolet (UV) light. Powder bed fusion (PBF) methods use fine powder as raw material, which is selectively melted with a laser beam (PBF-LB) or an electron beam (PBF-EB, for electricity conductive materials). Material extrusion (MEX) methods use solid filaments or granulate raw material, which is heated to a semi-molten state and extruded through a nozzle and deposited layer-by-layer to create a part (Bikas et al., 2016).

Depending on the AM method used, and geometry of the manufactured component, support structures may be needed in areas which have steep overhangs. Areas that have overhangs of 45 degrees or more are considered non-self-supportive during the manufacturing process, and may lead to failures in manufactured parts (Kállai et al., 2025). The support structures are added where needed to prevent the component from collapsing during the manufacturing process. The support structures can be created manually, or they can be realized through an overhang detection algorithm, which recognizes the critical places where the geometry is not self-supportive during manufacturing, and automatically suggests and creates the required support structures (Dobrzańska-Danikiewicz & Bączyk, 2024). By implementing self-supportive designs for AMed parts, requirements for support structures, which are laborious to remove during post-processing and use excessive material that is not needed for the part geometry, can be decreased (Kladovasilakis et al., 2025).

AM allows sub-millimetre detail resolutions for methods such as MEX and PBF (Shakibania et al., 2022), and even sub-micron resolutions through novel nano 3D printers, that work similarly to VPP methods (Khalaj et al., 2021; Liu et al., 2023; Pattison et al., 2022). Precision in details and dimensions allows the use of small and complex geometries in the design of parts fabricated with AM (Farazin et al., 2025). Dimensional accuracy, which is determined by comparing the geometry of the AMed part to the CAD dimensions (Roberson et al., 2013), depends on multiple

factors, such as geometry of the design, AM technology and machine used, and manufacturing parameters, such as choice of material, layer thickness, orientation of the printed part, support structures, and post-processing (Piedra-Cascón et al., 2024).

Overall costs of AM production have decreased, and the manufacturing speed has simultaneously increased, which supports the use of AM as a more cost-effective solution when compared to conventional subtractive or formative manufacturing methods (Farazin et al., 2025; Fratini et al., 2025). AM can be used to manufacture parts locally from raw materials as on-demand production (Khalaj et al., 2021), and it is widely used among many industries to create customized parts with intricate functional structures (Dobrzańska-Danikiewicz & Bączyk, 2024). For example, AM enables the use of structures that have functionality properties and mechanical performance required in aviation applications, where light weight and mechanical strength are both crucial requirements (Kladovasilakis et al., 2025). It can also be used to increase sustainability through prolonging product lifecycles, either by producing new spare parts on-demand, solving the problem of discontinued spare part production, or using AM directly for *in-situ* repairing of deformed or damaged components (Ford et al., 2015). AM is used for rapid prototype manufacturing from polymer materials, but it importantly has an increasing interest and number of applications among many industries. Recent studies have focused on increased material selection, larger number of applications for AM, and more accurate modelling of the AM process. (Dobrzańska-Danikiewicz & Bączyk, 2024). Increasing number of different usable materials, such as natural and synthetic polymers, metals, ceramics, composites and living cells, increases the possible use cases for AM in different industries (Dobrzańska-Danikiewicz & Bączyk, 2024; Farazin et al., 2025; Khalaj et al., 2021; Kladovasilakis et al., 2025). Materials used for AM should possess good manufacturability in AM, which is a factor of for example viscosity, flowability in molten state, and solidification behaviour (Ali et al., 2024; Farazin et al., 2025).

To assess the trend for using AM in the biomedical field, a keyword combination search was conducted on Scopus, illustrating an increased interest in AM of biomedical field. The keyword combinations and results are shown in Figure 2 and Figure 3.

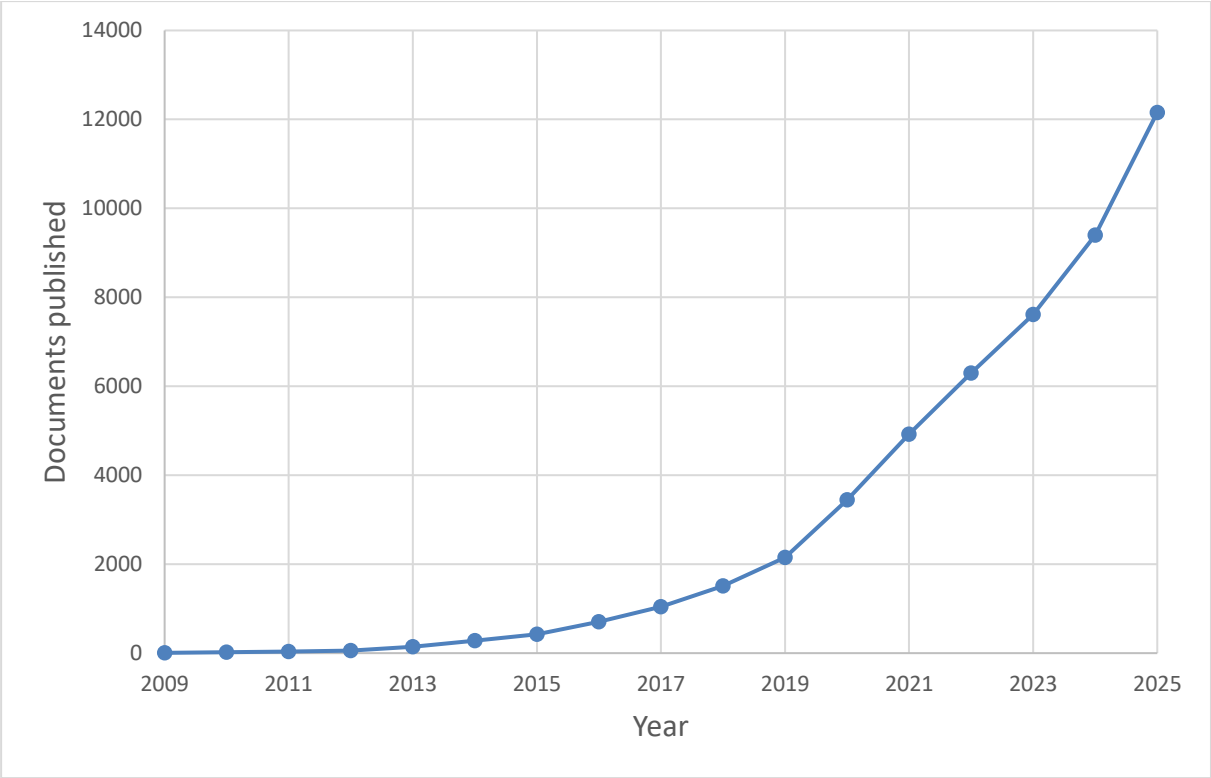


**Figure 2. Search results for "polymer" AND "additive manufacturing" AND "biomedical"**. The chart shows an increasing number of publications yearly from 2010 onwards, indicating growing interest towards additive manufacturing in the biomedical field.

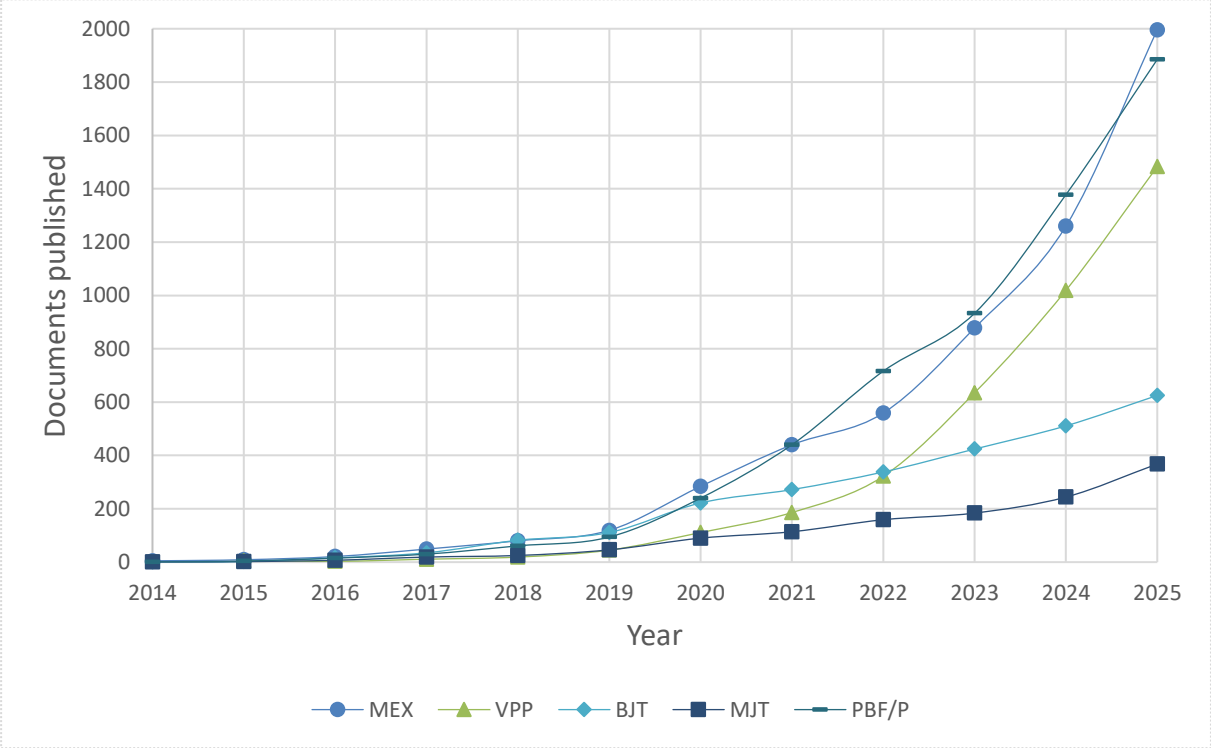


**Figure 3. Search results for different polymer AM methods.** The number of yearly publications for all of the polymer AM methods have increased, but at a different rate. Publications for methods such as PBF (of polymers) and MEX have increased more rapidly than for example binder jetting (BJT) and material jetting (MJT), indicating a higher interest for certain methods in biomedical applications than others.

There is an increasing trend of scientific publications per year for AM in biomedical applications, as can be seen in the keyword search results from Scopus in Figure 2 and Figure 3. PBF of polymers had the most publications, MEX came second, and VPP had the third most. Binder jetting (BJT) had fewer publications than VPP, and material jetting (MJT) had the fewest publications among the inspected keywords. Number of publications corresponds to the popularity of each AM method and the interest of the method in biomedical field, indicating that PBF, MEX and VPP are interesting, while BJT and MJT are less so.

## 1.1 Aim of the thesis

The thesis was done with MAF Medical Solutions Oy (Oulu, Finland), which focuses on medical device research and development.

The aim of the thesis is to determine a suitable AM method for producing small, complex biodegradable stent-like medical device prototypes. Limitations of different polymer AM methods considering their use in biomedical applications are studied. Critical requirements of the medical device are determined and based on the limitations of different AM methods and the listed requirements. The most suitable manufacturing method is determined as a result of the analysis.

A literature review is conducted for AM in biomedical field and medical device fabrication. Different AM methods and their suitability for manufacturing components for biomedical applications are reviewed. An emphasis is placed on understanding the limitations of different methods, and the criteria for the selection of the AM method in each case study is evaluated. Regulations and standards for medical devices and the use of AM methods in biomedical applications are studied.

The experimental part creates a two-component decision-making model, consisting of a decision-making tree which filters the unsuitable methods by guiding the user through a set of questions, representing a simulated decision-making process. The results are compared with the results of a quantified analytical hierarchy process (AHP) method, which is used for differentiating choices with multiple comparison criteria. Two different prototyping scenarios for a medical device prototype are studied: implantable or *in vivo* prototype, and a geometry-only functional prototype.

## 1.2 Research questions

Research questions were created for reviewing the use of polymer AM methods for medical device applications, to differentiate the polymer AM methods from each other for comparison depending on the requirements of the intended prototype use case, and to realize key limitations and advantages of polymer AM usage for medical device manufacturing or development were:

1. How is polymer AM currently utilized in fabrication, and research and development of medical devices?
2. What are the key advantages and limitations of different AM methods for medical device manufacturing?
3. Which criteria of a medical device prototype should be compared when considering the selection of a polymer AM method?
4. How can the most suitable polymer AM method be determined for a medical device prototype?

## 1.3 Description of the medical device prototype

The prototype studied in this thesis is a vascular implant, which closely resembles a vascular stent. It has a small thin-walled tubular geometry, with an intricate wall structure and details in both the inner and outer surfaces of the wall geometry. The device prototype is designed to withstand radial stress and expansion without breaking. The material has to conform to regulatory requirements for use within the human body, and it must biodegrade controllably within a pre-determined time period of 3-6 months.

## 1.4 Limitations for the thesis

As the medical device prototype studied in this thesis is a novel design with different functionality and target vascular environment compared to currently existing similar devices, there are no available scientific publications for the specific use case of the device for the literature review. The literature review therefore focuses on existing similar devices (vascular stents) that have somewhat simpler geometries compared to the design of the device prototype but have similar structure and properties in general.

# 2 AM in biomedical field

AM has become a manufacturing approach in the biomedical field, especially for small and complex biomedical devices which benefit from AM methods that have high manufacturing accuracy (Ali et al., 2024; Farazin et al., 2025; Kladovasilakis et al., 2025). Biomedical field uses AM for anatomical models for visualization and simulation of surgical procedures (Hong et al., 2023) (illustrated in Figure 4), dental applications, surgical guides, medical devices, implants, pharmaceuticals (Khalaj et al., 2021; Kladovasilakis et al., 2025), prostheses, orthopaedic implants (Gonçalves et al., 2021; Wang & Yang, 2021), vascular stents (Guerra et al., 2017; Khalaj et al., 2021; van Lith et al., 2016; Wang & Yang, 2021), and other scaffolds used for repairing soft and hard tissues inside the human body (Wang & Yang, 2021). The availability to control the porosity in the AMed structures leads to parts with less unintentional voids in the structure, which minimizes the possibility of growth of pathogens in narrow passages where the human body white cells cannot reach. This reduces the amount of inflammation, and therefore promotes the use of AM in biomedical devices and implants operating inside the human body (Kladovasilakis et al., 2025).

AM enables the design of more individualized biomedical devices to target patient-specific needs (Fratini et al., 2025; Gonçalves et al., 2021). Customizability and individualization of manufactured products is easier when comparing to conventional subtractive or formative manufacturing methods (Zhu et al., 2025). AM also allows rapid prototyping and design verification testing possibilities, as tooling changes are not necessary between development cycles, making the design changes during the development phase, and the application of product to markets an easier and faster process in the biomedical field (Ali et al., 2024; Khalaj et al., 2021; Mançanares et al., 2015).

Additive manufacturing can also be used in visualization, educative and training purposes. Hong et al. (2023) for example used AM to manufacture models based on real computed tomography data. The models used for surgical operation training are shown in Figure 4c-d**.**

.

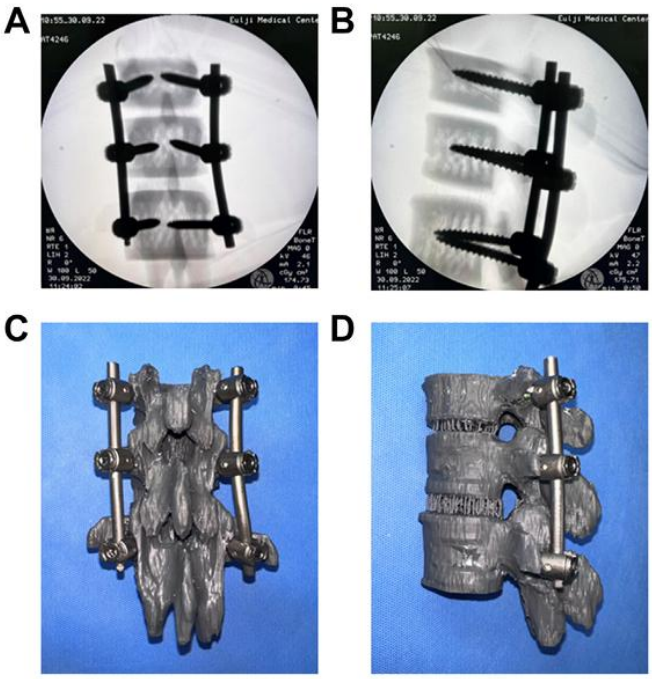


**Figure 4. Simulated surgery training model for pedicle screw fixation operation.** Sections a and b show the pedicle screws that are fixed to the model. Sections c and d show the AMed surgical training models based on real-sized computed tomography data acquired from a spine of a patient. Figure from Hong et al. (2023).

Figure 4c and 4d show the surgical simulation training model used in study by Hong et al., (2023). The effects of simulated surgical training done with AMed models based on real computed tomography scan data from patients were studied. The simulated surgical operation was pedicle screw fixation. The operation includes risks for causing nerve damage when inserting the pedicle screws seen in Figure 4a and 4b. The fixation operation requires precise orientation and placement to avoid nerve damage, and therefore training with a simulated setup is desirable pre-operation. It was found that training repetitions with the AMed models increased the accuracy of the procedures while simultaneously lowering the time taken for the procedure. (Hong et al., 2023)

AM for biomedical applications requires consideration for mechanical properties of the AMed part to fill any technical requirements of the application and withstand physiological stresses and conditions appearing inside the human body. It is also crucial that any products meant to be implanted inside the human body are biocompatible to minimize any adverse reactions, such as immunogenicity, inflammatory reactions, or toxicity, when in contact with living tissue or bodily fluids (Ali et al., 2024; Chartrain et al., 2018; Farazin et al., 2025). Wider selection of usable biocompatible materials increases the possible areas of application for AM in the

biomedical field (Kladovasilakis et al., 2025). Advances in biocompatibility and biodegradability of biomaterials that are usable for polymer AM have increased potential in applications requiring tissue regeneration, low inflammatory responses, and low immune responses (Zhu et al., 2025).

Biopolymers are biomaterials used for manufacturing medical devices in polymer AM (Ali et al., 2024; Wang & Yang, 2021). They can be divided into natural and synthetic polymers, hydrogels and polymer composites. Natural polymers are biocompatible and biodegradable through hydrolysis, which produces $CO_2$ and water (Ali et al., 2024; Rebelo et al., 2017). They have drawbacks, such as poor manufacturability and mechanical properties when used in AM (Ali et al., 2024; Farazin et al., 2025). On the other hand, advances in biocompatibility and biodegradability of polymer materials make them a good alternative to conventional materials like metals and ceramics in biomedical applications, such as implantable devices, if the mechanical properties of used polymers are sufficient considering the requirements of the application (Khalaj et al., 2021; Rebelo et al., 2017). Illustrations of use cases for metal and polymer materials are presented in Figure 5.

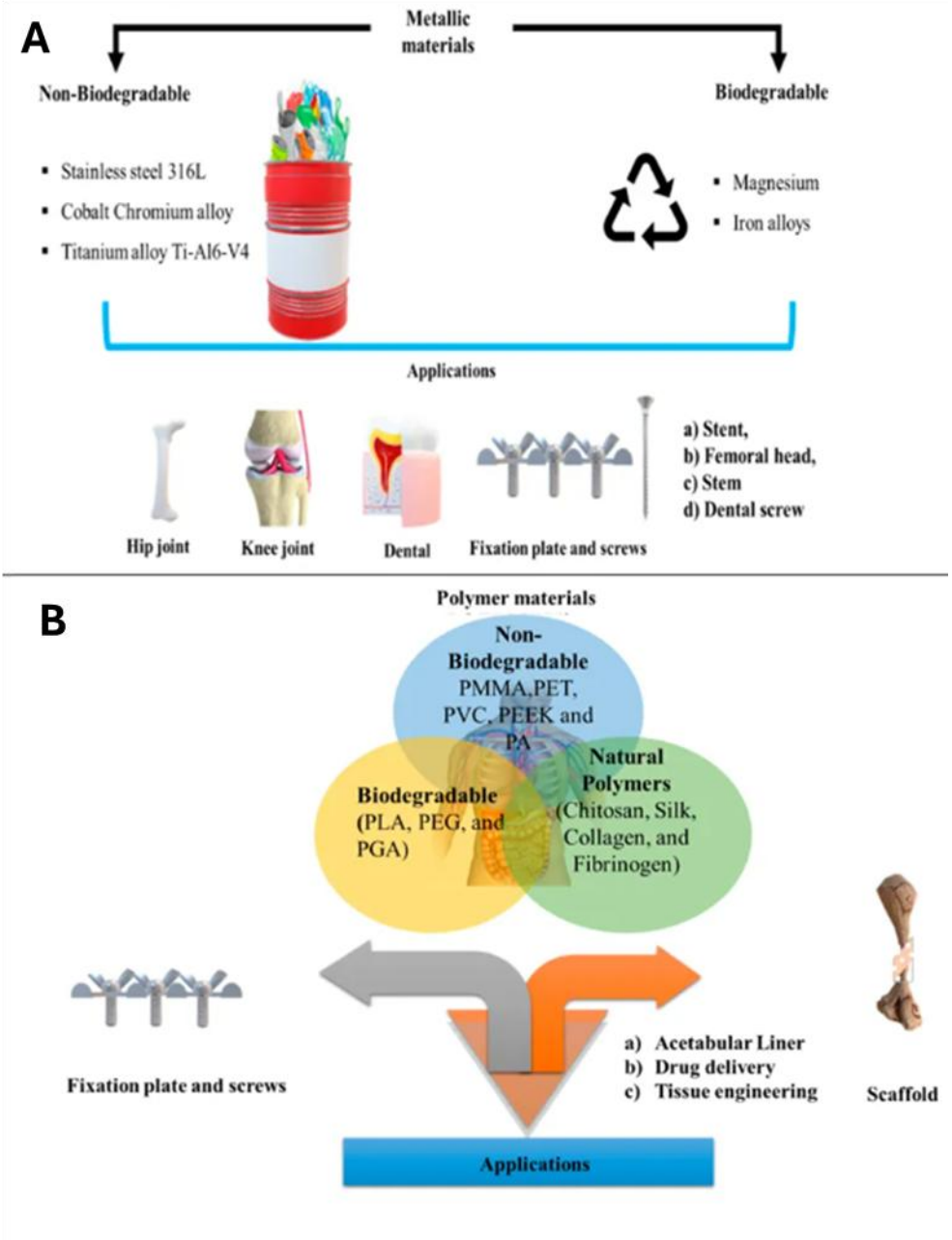


**Figure 5. Materials used for biomedical applications.** Section a shows examples of metals that are used for biomedical applications, and section b shows polymer materials used for biomedical applications. Figure taken and modified from S. et al. (2024).

As seen in Figure 5a, metals are preferable for permanent implants which are subjected to high loads, for example knee joints or dental implants (S. et al., 2024). Biodegradable natural polymers shown in Figure 5b are a better choice when used in temporary medical devices, as the need for secondary surgical procedures for removing the device are not needed after the treatment, and the inflammatory responses are lower (Rebelo et al., 2017; S. et al., 2024). The biodegradation byproducts of biodegradable polymers are non-inflammatory, making natural biopolymers a good material choice for temporary medical devices. Metals for example cause

inflammatory responses around the implanted areas when used in long-term implantation applications due to ion leeching (Rebelo et al., 2017; S. et al., 2024). Synthetic polymers shown in Figure 5b allow the control of physical and chemical properties which allows better mechanical properties and slower degradation for the product (Ali et al., 2024). There are however some concerns about biocompatibility and degradation byproducts for synthetic polymers, making them less desirable alternative to natural biopolymers for use in implantable biomedical applications (Ali et al., 2024; Rebelo et al., 2017).

Polymer materials used for AM in medical applications include polylactic acid (PLA), polyglycolic acid, poly(lactic-co-glycolic) acid (PLGA), polycaprolactone (PCL), medical-grade silicone, poly(l-lactide-co-e-caprolactone), and polyetheretherketone (Ali et al., 2024). These polymers are suitable due to their non-toxicity, biodegradability and biocompatibility (Ali et al., 2024). Many polymers, for example PCL, PLA and polyamides (PAs), are good materials for polymer AM methods such as PBF and MEX, as they are chemically stable. They have low melting and glass transition temperatures compared to metals or ceramics, so they require less powerful heat sources to be processed, reducing the required energy when manufacturing products (Ali et al., 2024; Khalaj et al., 2021). PLA and PCL have also already shown great biocompatibility with the human body and are already used for many biomedical applications (Kladovasilakis et al., 2025).

The material used for manufacturing products for biomedical applications should endure standard sterilization methods, as sterilization is often a requirement when manufacturing biomedical devices, especially implantable devices. Sterilization, such as autoclaving, gamma irradiation, or ethylene oxide gas sterilization, causes polymer degradation, which decreases the mechanical properties and integrity of AMed parts (Ali et al., 2024; Farazin et al., 2025; Khalaj et al., 2021). PLA for example loses molecular weight when subjected to gamma or electron beam irradiation, with a higher dosage of irradiation corresponding to a larger loss of molecular weight (Benyathiar et al., 2021). The drop in molecular weight decreases tensile strength, elongation at break, and elastic modulus, which causes embrittlement of the material (Benyathiar et al., 2021; Krug et al., 2024). Melting temperature of the polymer material also decreases (Benyathiar et al., 2021), and the hydrolysis biodegradation for materials such as PLA and PLGA is accelerated (Braghirolli et al., 2011).

Biodegradable AMed parts must lose their mechanical properties in a predictable and controlled manner and degrade within a predetermined timeframe to be safely used inside the human body (Ali et al., 2024; Chartrain et al., 2018). Unpredictable loss of mechanical properties can lead

to mechanical failures, which leads to risks concerning the operational safety and functionality. The biodegradation must also be rapid to avoid excessive foreign body reactions and inflammatory responses caused by the implanted device while it is implanted inside the human body (Ali et al., 2024).

Medical devices need to follow requirements set by regulatory authorities, such as the U.S. Food and Drug administration (FDA) and European Commission (EC). EC for example divides medical devices into five categories as follows: 1) models for preoperative planning, 2) tools, instruments and parts for medical devices, 3) inert implants, 4) medical aids, supportive guides, splints and prostheses, and 5) biomanufacturing. Medical devices are further classified into I, IIa, IIb and III inside each category according to their risk levels. Especially for Class III high-risk devices, such as medical stents implanted to the human body through a surgical procedure, strict regulations must be followed (Khalaj et al., 2021).

EC has recognized advantages for the use of AM in medical device applications due to for example reduced waste material and healthcare costs in general and improved physiological outcomes for patients. The FDA has updated its regulations on AM technologies, as the use of AM in in medical device manufacturing has increased. FDA guideline is split into design and manufacture consideration section, and device testing consideration section. Device testing considerations include for example technical considerations that should be assessed on quality system requirements for the medical device. Quality system regulations and current good manufacturing practice specifications must be addressed for any medical device. (*Technical Considerations for Additive Manufactured Medical Devices - Guidance for Industry and Food and Drug Administration Staff*)

New materials must also go through a process to be proved safe and effective, or comparable to a material that is already used in a medical device. Material and manufacturing process receives clearance from the FDA separately for the medical device (risks versus benefits), raw material (biocompatibility), and manufacturing method, including for example the use of parts made by AM or the AM method used for manufacturing the device (Khalaj et al., 2021). Out of all available AM methods, only some are usable for biomedical applications, mainly due to biocompatible and biodegradable material availability and strict process conditions (Farazin et al., 2025).

ISO 10993 standard categorizes the level of contact a medical device has with the human body, and evaluates proper chemical, physical, toxicological, electrical and morphological

characteristics. Any medical device or material used in the device needs to undergo biocompatibility evaluations based on the level of contact with the human body (ISO 10993-1:2018). It is therefore feasible to select a readily accepted material which can be used in AM when designing a new medical device, as the validation process for the medical device becomes shorter (Farazin et al., 2025).

# 3 Biodegradable Stents

Stents are used in locations inside the human body where support, passage widening, or repositioning is required. Stents can be used for example in the heart, arterial and venous system, ureter, urethra, oesophagus, bile duct, prostate, nasal cavity and vagina. The requirements in shape or geometry of the stent may vary depending on the complexity of the treatable area (Khalaj et al., 2021). Different stent designs and design elements are illustrated in Figure 6.

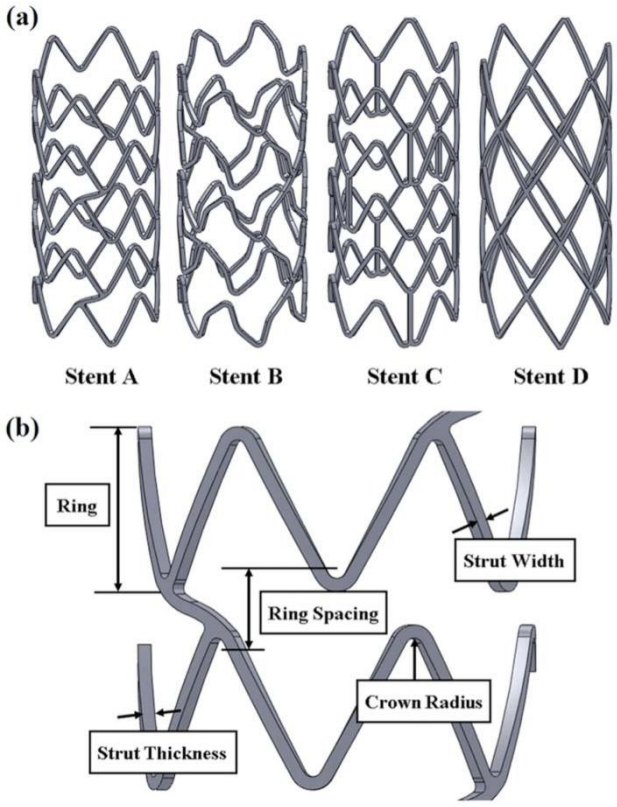


**Figure 6. Examples of stent wall structures and naming of structural elements of stents.** Section a shows different wall structure designs for stent prototypes. Section b shows the different design elements for the wall structure. Figure from Hsiao et al. (2014)

Figure 6a shows different wall structure designs for coronary stents. Different complex geometries and structures can be manufactured and tested rapidly to determine the best design for a specific treatable area of the stent, when using AM methods instead of conventional subtractive or formative methods. Stent design parameters can be seen in Figure 6b. Strut thickness is one key consideration for stents, because it affects the contact pressure between the stent and the inner layers of arteries (Khalaj et al., 2021). Excessive contact pressure leads to perpetuating restenosis, which is a reduction of the diameter of blood vessels, eventually leading to blockages of blood flow (Omeh & Shlofmitz, 2025). Damage to the endothelium and

deeper layers of arteries causes platelet activation, which can lead to thrombosis or clotting of the artery (Costa et al., 2018; Khalaj et al., 2021).

One common application for stents are cardiovascular diseases (CVDs). CVDs are very common and are the reason for up to half of deaths in Europe. They occur due to fatty substances gathering on the walls of an artery, decreasing the lumen area of the vein, which means the inner cross-section of the vein, causing blockages of blood flow to the heart (Burt & Hunter, 2006; Kiousis et al., 2009). Minimally invasive balloon angioplasty with stenting is a relatively safe and effective way to treat CVDs (Kiousis et al., 2009; Kladovasilakis et al., 2025).

A stent mounted to a balloon catheter (as seen in Figure 7 a-c) is inserted into an artery and guided to the area of blockage. The stent is then expanded with the balloon to press the fatty substances towards the walls of the artery to increase the lumen area and restore the blood flow. The balloon is then deflated, and the catheter is removed with the stent remaining *in situ,* degrading slowly over time (Kladovasilakis et al., 2025).

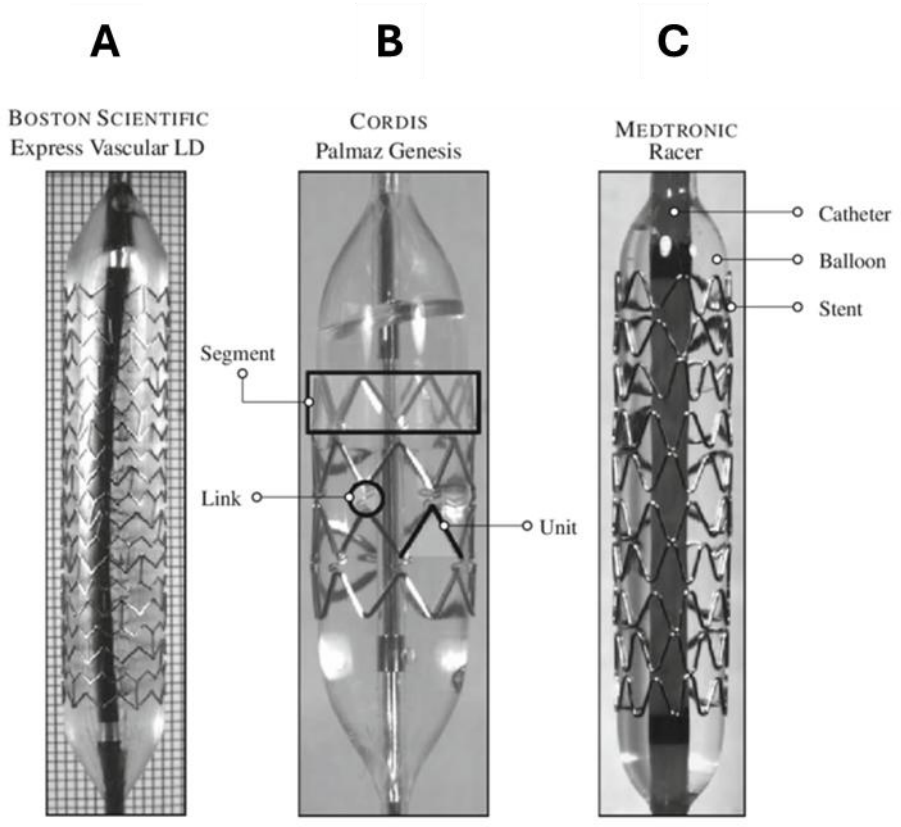


**Figure 7. Balloon expandable stent-catheter delivery systems.** There are stents from three different manufacturers. Section A shows a stent by Boston Scientific, section B shows a stent by Cordis, and section C shows a stent by Medtronic. The stents are inserted onto a catheter, which are in an expanded state. Figure from Kiousis et al. (2009).

As seen in Figure 7 a-c, a balloon expandable stent-catheter delivery system consists of a balloon, a catheter and a stent mounted on top of the balloon. The catheter is a long wire-like component used to steer the stent to a desired location inside a vein. Once the catheter is in place, the balloon is expanded, as seen for all the balloon expandable stent-catheter delivery systems in Figure 7 a-c.

Despite the effectiveness of stent treatments for CVDs, stent placement includes a number of complications. A stent is mechanically in contact with the inner wall (or endothelium) of the vein. The contact causes not only inflammation due to foreign body reactions but also mechanical trauma. The trauma is associated with improper implantation techniques and stent design. (Kiousis et al., 2009)

Thrombosis (blood clot formation) or hyperplasia (accelerated cell production) may also occur after the implantation (van Lith et al., 2016). Stent related thrombosis is especially problematic as it is associated with high rates of mortality and morbidity, and often leads to conditions such as nonfatal myocardial infraction or cardiac death (Modi et al., 2025). Stent thrombosis occurs due to small cross-section (smaller than 5 $mm^2$) of the stent, incorrect position or orientation of the stent, plaque prolapse (tissue extruding from between the stent struts to the inner area of the vein, illustrated in Figure 8), edge dissection (tear in a wall of an artery caused by the stent or the placement operation), or in stent restenosis (blockage of blood flow caused by the stent) (Burt & Hunter, 2006; Kladovasilakis et al., 2025; Modi et al., 2025).

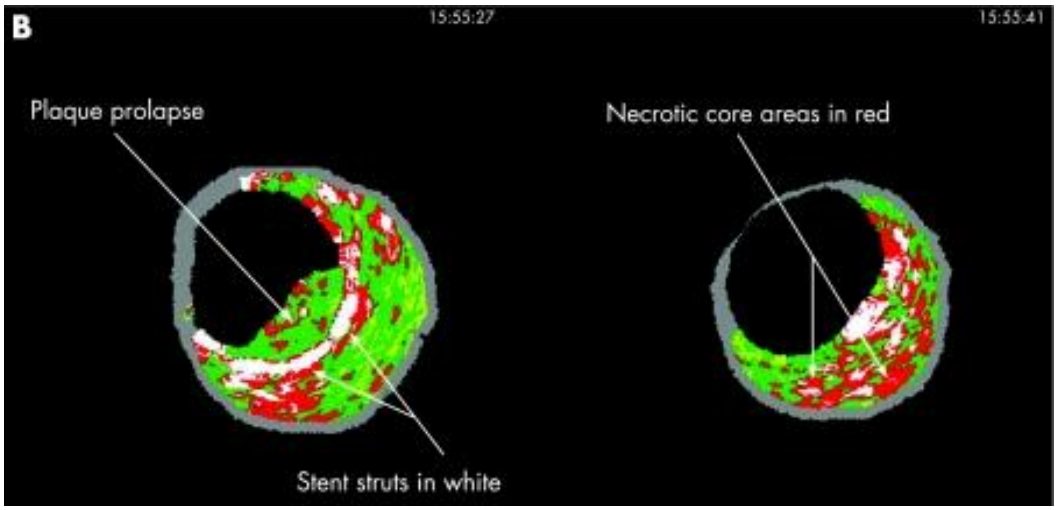


**Figure 8. Plaque prolapse.** The plaque prolapse can be seen as the green and red coloured area inside the cross-section enclosed by the stent struts. Figure from Tsui & Lau (2007).

Figure 8 shows one of the stent thrombosis related occurrences, plaque prolapse, where plaque extrudes through the stent struts from the surface of the vein. This causes blockages of blood flow by decreasing the lumen area of the vein. It occurs due to stent implantation circumstances, for example the use of post-dilatation balloon and the size and maximum applied pressure during inflation of the balloon (Umemoto et al., 2017).

Stents can be coated with an antiproliferative medicine, which slows down the cell regrowth and healing of the blood vessel where the stent is placed (Costa et al., 2018; Kiousis et al., 2009). Using stents coated with antiproliferative medicine, called drug eluting stents, decreases the occurrence of stent related restenosis (Costa et al., 2018; Khalaj et al., 2021; Kiousis et al., 2009).

Any foreign material left inside the vein from the stents cause adverse reactions inside the human body (Flege et al., 2013; Guerra et al., 2017; van Lith et al., 2016). Stents made from permanent materials such as metals, ceramics, or non-degradable polymers remain *in situ* even after the healing of the vessel has been completed (Guerra et al., 2017). Remaining materials can cause mechanical traumas to endothelium (Costa et al., 2018; van Lith et al., 2016). The use of permanent materials for implants may also be not preferable if the patient is young, as future growth of the arteries is expected, or when there may be a further need for surgeries (Kladovasilakis et al., 2025).

Fully bioresorbable stents (BRSs) are an alternative for conventional permanent metal stents, and have shown efficacy and safety of use in coronary artery disease patients (Khalaj et al., 2021; van Lith et al., 2016). BRSs get gradually absorbed by the human body and leave no permanent foreign materials at the site of implantation after complete absorption (Guerra et al., 2017; Khalaj et al., 2021; van Lith et al., 2016). The complete absorption should occur within 6-9 months after placement to prevent excessive inflammation (Flege et al., 2013), when supports are no longer required due to healing of the treated area, such as an artery (Guerra et al., 2017; van Lith et al., 2016). Optimally the degradation time should be long enough to provide sufficient support in the treatable area, and the degradation should occur at a rate which decreases the mechanical strength of the stent at a same rate that the treatable area cell production increases the strength of the treatable area (Chartrain et al., 2018). Usage of biodegradable polymers has advantages in reduced inflammatory reactions due to weaker foreign body reactions (Flege et al., 2013; Khalaj et al., 2021; van Lith et al., 2016).

Figure 9 illustrates different wall designs of common commercial BRSs.

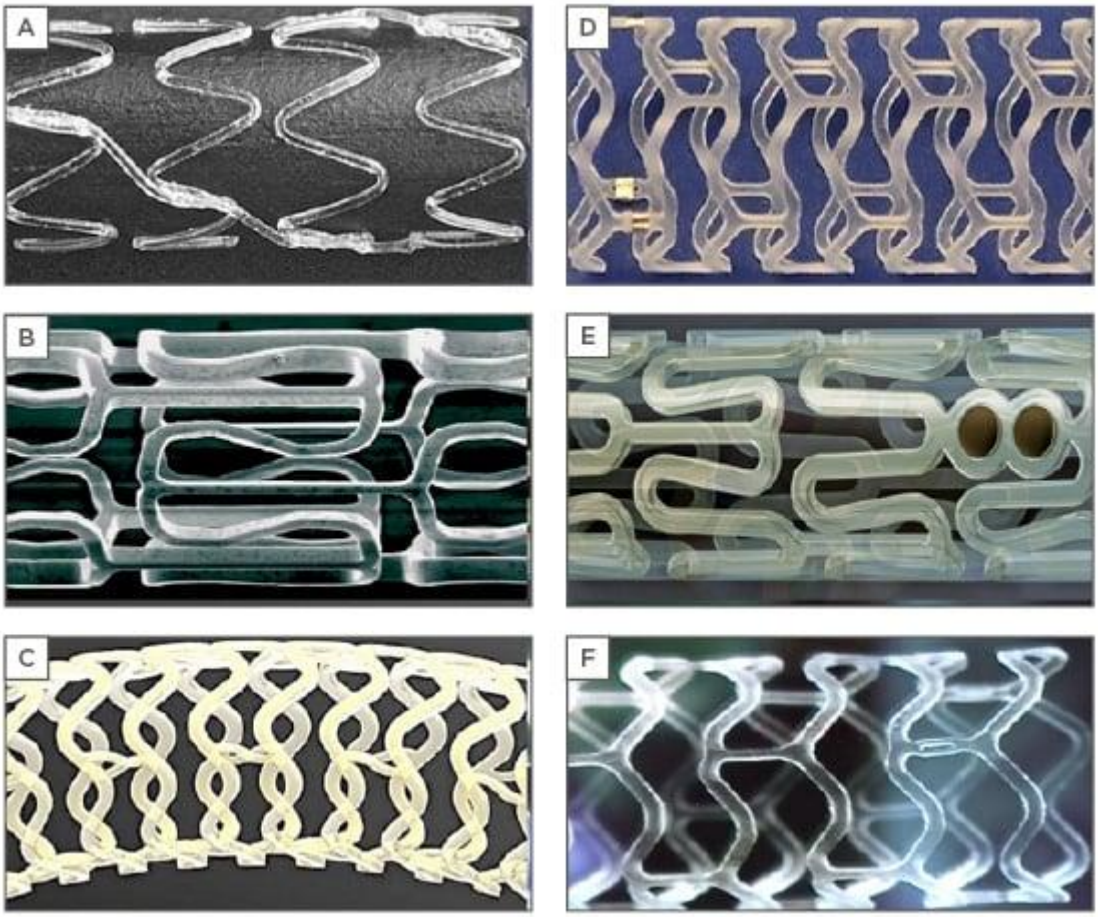


**Figure 9 Bioabsorbable stent designs.** Section A is the Igaki-Tamai stent made from PLLA by tube extrusion and laser cutting. Section B is a bioabsorbable metal stent design. Section C is Fantom stent by REVA Medical Inc., made from polycarbonate and coated with anti-proliferative drug. Section D is DESolve BRS by Elixir Medical, made from PLA and coated with antiproliferative drug. Section E is ABSORB vascular by Abbott Vascular, made similarly to Igaki-Tamai by tube extruding and laser cutting PLLA. Section F is Fortitude by Amaranth Medical, also made from PLLA. Figure from Goel et al. (2017).

Igaki-Tamai stent, shown in Figure 9a, was the first BRS implanted in human patients, made from poly l-lactic acid (PLLA) material (Flege et al., 2013; Iqbal et al., 2013). PLLA degrades through hydrolysis of bonds between repeating lactide units, and produce lactic acid and oligomer fragments, which are metabolized by the human body into $CO_2$ and water (Flege et al., 2013; Khalaj et al., 2021; van Lith et al., 2016). The Igaki-Tamai stent performed well in human patients, but the implantation was found to be a challenging process (Flege et al., 2013). The Igaki-Tamai stent is completely resorbed by the human body within 2 years of implantation (Iqbal et al., 2013).

ABSORB vascular stent made by Abbott, shown in Figure 9e**,** is the most used bioabsorbable stent (Goel et al., 2017). ABSORB has received Conformité Européene (2010) and FDA approval (2016) for coronary artery use (Goel et al., 2017; Khalaj et al., 2021). The ABSORB

stent provided sufficient mechanical support for the treatable artery for a duration of 6 – 12 months and was fully resorbed in the human body within 2 – 3 years of implantation (Iqbal et al., 2013; Khalaj et al., 2021).

Both, the Igaki-Tamai (Fig. 9a) and ABSORB (Fig. 9e) stents, were manufactured by fabricating cylindrical PLLA tubes, and laser cutting the intricate stent wall structure (strut) pattern from the cylinders (Khalaj et al., 2021). The use of subtractive methods in this case leads to larger amounts of waste material when comparing to additive manufacturing methods. Medical grade materials are expensive compared to non-medical grade materials, making the material saving capability of AM methods valuable in biomedical applications (Fratini et al., 2025; Guerra et al., 2017). By utilizing AM methods, stent manufacturing could also be performed locally where the stent is needed, for example in a hospital, reducing pollution, delivery times, and economical costs, due to logistics (van Lith et al., 2016).

AM has shown promise in solving problems related with stent design and manufacturing (Guerra et al., 2017). It has advantages in solving geometrical issues with stent design, such as inappropriate strut sizing, which lead to stent-related complications (Fratini et al., 2025; Khalaj et al., 2021; Kiousis et al., 2009). A patient may also have non-typical vessel geometry, which is often problematic in endovascular surgeries. AM supports the concept of patient-specific stent design, countering the problem of non-typical vessels the patient may have (Fratini et al., 2025; van Lith et al., 2016).

Despite the advantages of using AM methods for stent fabrication, implementation of polymer AM methods for fabrication of stents used inside the human body has so far been small-scale. AM has mostly been used in single patient cases where the need of intervention or treatment has been urgent, or the application is low risk. Therefore, the AM process used for medical device manufacturing has not had to undergo strict regulatory procedures, set by EC or FDA, for use in live patients. While proof-of-concept stents and prototypes of stents have been successfully created with AM methods, extensive research with verification of biocompatibility, and *in vivo* biodegradation profile is required, as enzymatic responses within the human body are known to accelerate the degradation and resorption of biopolymers.

Resolution capabilities of some AM machines are insufficient for creating thin wall structures of less than 300 µm in diameter, limiting the use of certain methods for fabricating stent-like medical devices. For example, the nozzle diameter restrictions determine the smallest possible detail accuracy for MEX machinery, and for laser or UV beam-based technologies such as PBF-

LB/P and VPP, the beam power and diameter, and solidification behaviour of the material affect the resolution capability. (Khalaj et al., 2021)

Another problematic property for AMed stents is surface smoothness. For polymer-based stents, surface smoothness is difficult to achieve through AM methods based on layer-by-layer deposition of material (Khalaj et al., 2021). Mechanical strength of AMed stents is also questionable, requiring proper material and AM method selection, and optimization of manufacturing parameters (Ali et al., 2024).

# 4 Polymer AM methods for stent-like medical device manufacturing

## 4.1 Material extrusion

MEX methods use solid thermoplastic filaments or granulate as raw materials (Ali et al., 2024; Bikas et al., 2016; Farazin et al., 2025; Yue Ma et al., 2024; Zhu et al., 2025). The process is illustrated in Figure 10.

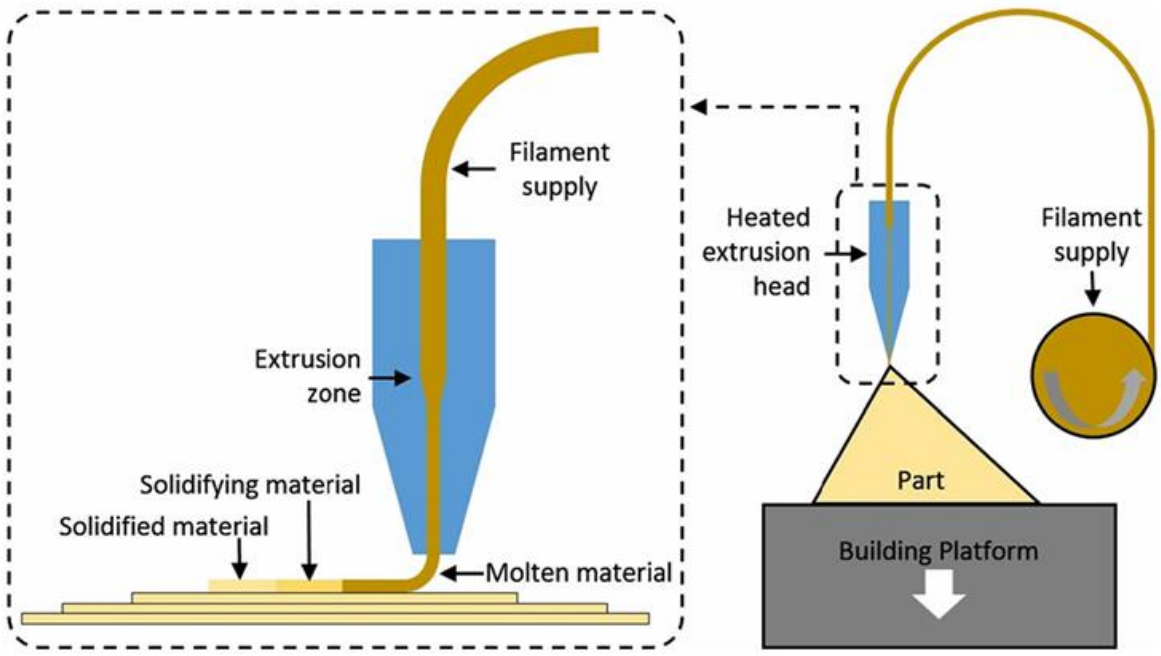


**Figure 10. Visualisation of a material extrusion process**. Solid thermoplastic filament (filament supply) is supplied to the heated extrusion head (blue), where the heat is applied to the polymer to change it to a semi molten state. The narrowing part of the heated extrusion head is the nozzle, through which the material is applied on top of the previous layer of solidified polymer on the building platform. After a layer is complete, the build platform lowers, and another layer is added on top of the last applied layer until the part is complete. Figure from Bikas et al. (2016).

As seen in Figure 10, the material is first supplied to the heated extrusion head of the MEX machine. Heat is applied to the thermoplastic material as it reaches the nozzle, until the temperature rises just above the characteristic melting point of the polymer material (Bikas et al., 2016). The material phase changes into a semi-liquid state as it travels through the nozzle of the MEX machine (Ali et al., 2024; Bikas et al., 2016; Farazin et al., 2025; Yue Ma et al., 2024; Zhu et al., 2025). The semi-liquid polymer is selectively deposited on the build platform of the AM machine by x- and y-directional movement of the nozzle (Farazin et al., 2025). After the polymer layer has cooled down and solidified, the build platform moves down in z-direction,

and the subsequent layer is selectively applied on top of the previous one. The process is repeated until the part is complete (Bikas et al., 2016; Farazin et al., 2025; Zhu et al., 2025).

Figure 10 shows a MEX process which uses a filament material feedstock. The filament supply could also be replaced with a feeding system for granulated or pelletized polymer material. The material is cooling down (transition from darker yellow to lighter yellow) after being deposited on top of the previous layer on the build platform to form a solid layer. Figure 10 also shows the method MEX uses to create the shape of the printed part in z-direction by changing the cross-section, in this case to a smaller one than the previous layer. The layer-by-layer deposition of material leads to a step-like structure between the individual layers, which leads to a rough surface quality for the manufactured parts.

Key manufacturing parameters for MEX include layer thickness, material selection, nozzle temperature, printing speed (the flow speed of the material and the nozzle movement speed on the build platform), and infill density (the percentage of material per volume unit of the part) (Spina, 2025; Zhu et al., 2025). MEX is capable of producing minimum feature sizes from as low as 60 µm to 600 µm depending on manufacturing parameters such as layer height, nozzle movement speed and material selection (Corrado et al., 2025). The smaller feature sizes are possible in the printing direction, controlled by the layer height. Manufacturers such as Bambu Lab or Ultimaker suggest the use of 0.2 or 0.4 mm nozzle diameter for materials like PLA, which limits the minimal feature size in xy-direction (on the build platform) to 200 – 600 µm.

MEX is the most commonly used AM method (Ali et al., 2024; Dobrzańska-Danikiewicz & Bączyk, 2024), and has advantages in accessibility of the machinery and relative simplicity of the AM process (Farazin et al., 2025; Yue Ma et al., 2024; Zhu et al., 2025). MEX machinery is generally cheaper when comparing to machinery in other methods like VPP and PBF. Simplicity of the manufacturing process, low prices of MEX machinery and operational costs make MEX the cheapest AM method for manufacturing costs per product (Dobrzańska-Danikiewicz & Bączyk, 2024; Farazin et al., 2025; Roberson et al., 2013). MEX has been used for rapid prototyping for decades, but with an increasing interest in commercial product manufacturing, including biomedical applications such as implants (Bouzaglou et al., 2023).

MEX methods are compatible with many thermoplastic materials, such as FDA-approved biocompatible and biodegradable polymers PLA, PCL (Bouzaglou et al., 2023; Farazin et al., 2025; Singh et al., 2025; Yue Ma et al., 2024; Zhu et al., 2025), PLGA (Kulker et al., 2025), polyethylene glycol, and polyhydroxyalkanoates (Zhu et al., 2025). PLA especially has suitable

material properties for use with MEX methods due to its good flowability in molten state and solidification behaviour (Zhu et al., 2025). Compatibility with biodegradable and biocompatible materials enables the use of MEX for manufacturing components for biomedical applications. Biomedical field uses MEX for example for manufacturing patient-specific implants, prosthetics, tissue-engineering scaffolds, and drug delivery systems (Kulker et al., 2025; Zhu et al., 2025).

Drawbacks for using MEX as a manufacturing method for biomedical applications include poor mechanical properties, for example tensile strength, when comparing to parts fabricated with subtractive or formative manufacturing methods (Ali et al., 2024; Bouzaglou et al., 2023; Farazin et al., 2025). Poorer mechanical properties for parts created with MEX methods occur due to low adhesion between individual layers of the manufactured part, which leads to structural weaknesses (Zhu et al., 2025). The mechanical properties of parts manufactured with MEX are also non-isotropic as the layer adhesion is weaker than the strength along a single layer (Bouzaglou et al., 2023; Spina, 2025). This limits the use of MEX especially for load-bearing applications (Ali et al., 2024). MEX also has lower dimensional accuracy when comparing to other AM methods (Ali et al., 2024; Bouzaglou et al., 2023; Spina, 2025). Fixed nozzle size and layer-by-layer deposition of the material can make fine details (smaller than the nozzle size) impossible to manufacture (Spina, 2025).

Dimensions are also affected by for example the warping of the printed part due to uneven cooling of the layers, which leads to uneven layer formation (Zhu et al., 2025). Inherent poor surface quality caused by stair-step structures between layers (as seen in Figure 10) is problematic for medical devices, and may lead to need of additional chemical coating or mechanical post-processing steps (Farazin et al., 2025; Park et al., 2015; Yue Ma et al., 2024; Zhu et al., 2025). The surface quality can also be affected by altering the manufacturing parameters of the MEX machine. Parameters such as nozzle temperature and flow speed of the material, and layer thickness have an effect of the surface roughness in parts fabricated with MEX AM methods (Spina, 2025). Effects of layer thickness on surface quality and porosity of the structure are visualized in Figure 11.

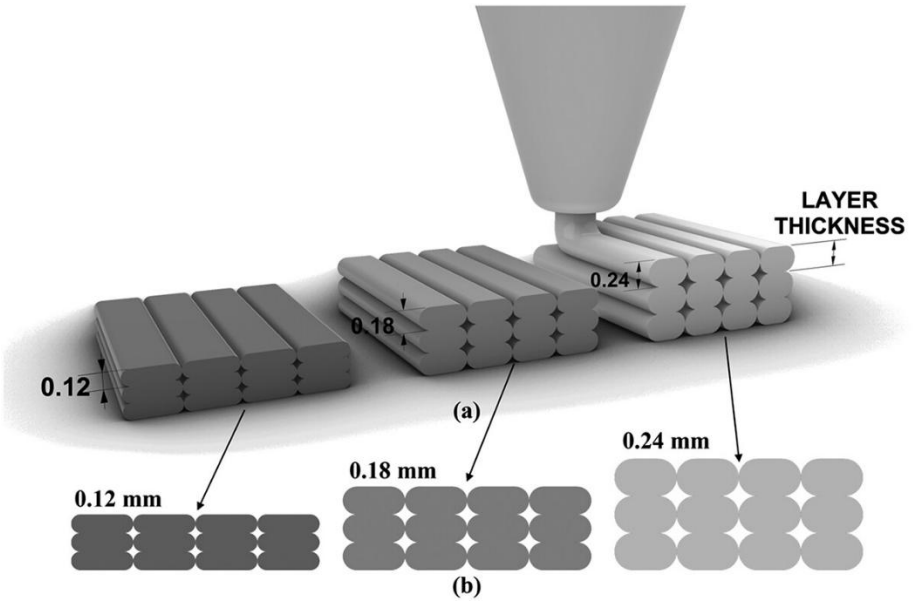


**Figure 11 Visualized effect of layer thickness on the manufactured part.** Increased air cavities between individual strands on each layer can be seen from 0.12 mm to 0.24 mm layer thickness.. Figure from Singh et al. (2025)

Figure 11 illustrates the effect of layer thickness for a part manufactured with material extrusion. Larger layer thickness increases the size of air gaps in the cross-section when comparing to similar structure with smaller layer thickness. The area of air cavities is inversly proportional to mechanical strength of the manufactured part. For this reason, the larger layer thicknesses should also be avoided when considering the mechanical strength of the part (Bianchi et al., 2022). While increasing the density, mechanical strength and interlayer fusion of the manufactured part, smaller layer thickness also contributes to a smoother surface finish, which can also be seen in Figure 11 with the 0.12 mm layer thickness having a smoother surface than the 0.18 mm and 0.24 mm layer thicknesses (Singh et al., 2025).

Singh et al. (2025) studied the effect of processing parameters on parts manufactured with MEX method from ABS filaments. Inspected parameters included layer thickness, and printing speed. It was found that, for commercial ABS filaments, 0.2 mm layer thickness contributed the lowest surface roughness. 0.1 mm layer thickness was found to increase the roughness due to poor inter-layer fusion. Larger than 0.2 mm layer thicknesses increased the roughness again as illustrated in Figure 11. The printing speed parameter had lower surface roughness for commercial ABS with low (40 mm $s^{-1}$) and high (60 mm $s^{-1}$) values, and a peak roughness in the middle (50 mm $s^{-1}$). Lower speeds lead to increased bonding time, which leads to a smoother layer forming. While higher speeds lack the bonding time, reduced material buildup on the manufactured part and improved flow of extruded material produce a smooth surface finish.

The middle speed was found to have issues with both the molten material flow and insufficient layer bonding, leading to a rougher surface finish overall.

Park et al. (2015) successfully fabricated a bioresorbable vascular stent using pelletized PCL material as feedstock for a customized MEX setup, illustrated Figure 12.

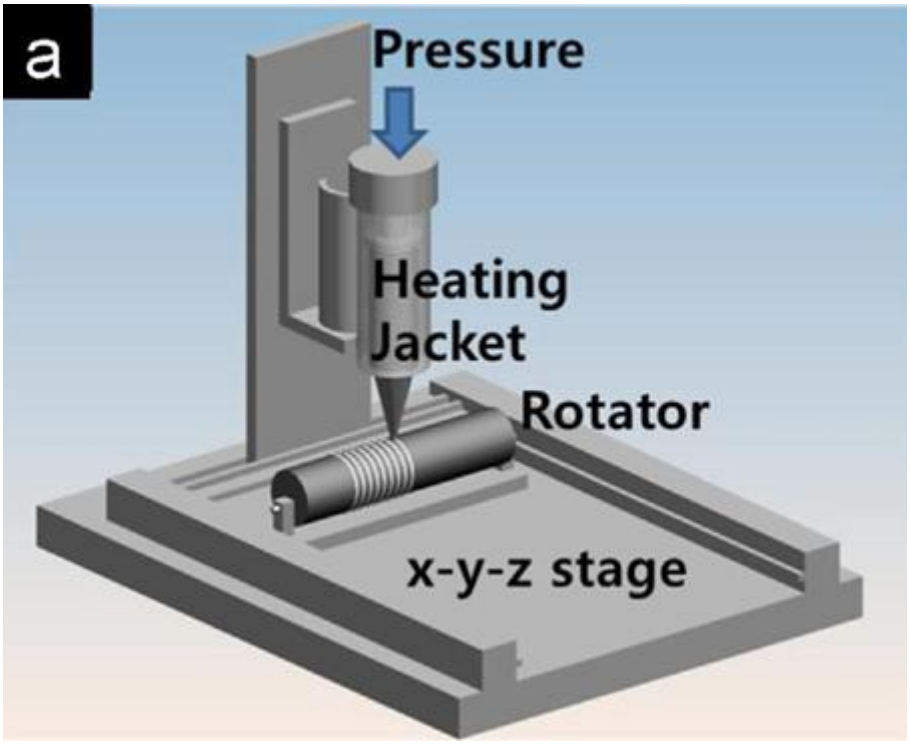


**Figure 12. Custom MEX setup used by Park et al. (2015).** Park et al. used the illustrated setup for manufacturing vascular stents by extruding the material on top of a rotating cylinder. Pressure is applied on top of the nozzle unit, through which the semi-molten thermoplastic material is extruded on the cylinder. By rotating and moving the cylinder, the intricate wall structure of the stent is fabricated on the surface of the cylinder.

As seen in Figure 12, the extruding was executed on top of a rotating cylindrical shaft (rotator), using a wall thickness of 300 µm, and 1.3 mm spacing between individual struts. To address the rough surface finish, inherent to MEX methods, the manufactured stents were coated with an immunosuppressive sirolimus drug, which was mixed together with PLGA. The coating was able to smooth the stair-step structures between the manufactured part layers, and the resulting surface smoothness was comparable with uncoated stents manufactured using conventional subtractive manufacturing methods. (Park et al., 2015)

Guerra et al. (2017) used a similar setup as seen in Figure 12, utilizing PCL filament as raw material rather than pellets like Park et al. (2015), for fabricating a BRS with a MEX method by extruding the PCL on top of a heated rotating mandrel.

## 4.2 Vat photopolymerization

Vat photopolymerization (VPP) methods use liquid resins as raw material (Ali et al., 2024; Bikas et al., 2016; Khalaj et al., 2021) The method works by changing the phase of the liquid resin to solid inside the vat by illumination of a specific wavelength (Ali et al., 2024; Bikas et al., 2016; Bosch et al., 2025). VPP includes several different techniques for curing the resins. Commercial names such as stereolithography (SLA) (Yue Ma et al., 2024; Zhu et al., 2025), Digital Light Projection (DLP) (Yue Ma et al., 2024; Zhu et al., 2025), and continuous liquid interface production (CLIP) (van Lith et al., 2016), all fall under the category of VPP AM methods. They have different approaches for solidifying the resin, but the fundamentals are similar. In this thesis, they will all be considered broadly as VPP methods but a description of the different method operating principles is provided within this chapter. Commonly the liquid resin is cured with an irradiation source, for example a laser beam or a projected UV light source, as shown in Figure 13 (Bikas et al., 2016; Khalaj et al., 2021).

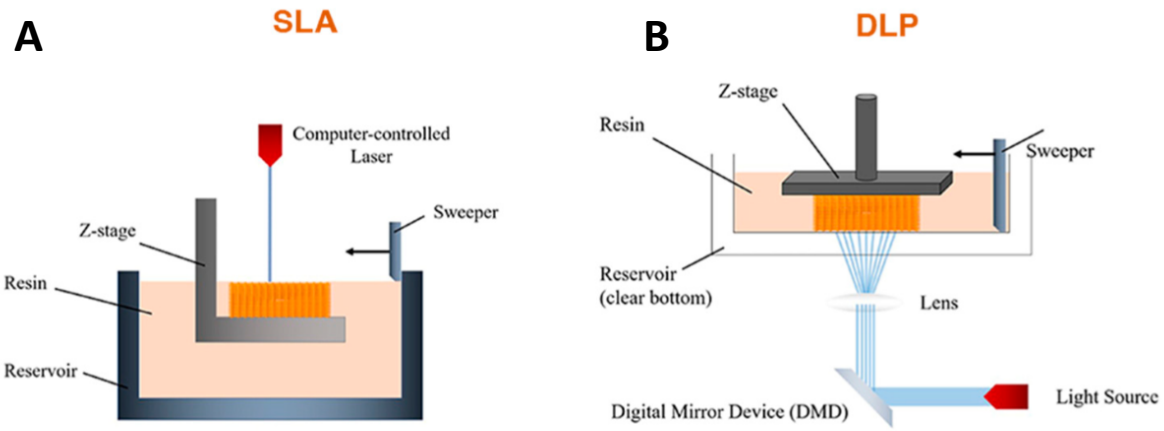


**Figure 13 Differences with operating procedures of different VPP methods (SLA and DLP).** Key difference between the methods is the illumination method of the resin inside the reservoir. Section A shows how SLA operates by controlling the movement of the beam source (computer-controlled laser), creating a solid layer on the build platform (z-stage). DLP is illustrated in section B. DLP creates a planar projection on the build platform (z-stage) by controlling individual mirrors of the DMD, solidifying the entire layer of the model simultaneously. Figure from Gonçalves et al. (2021).

Figure 13 illustrates the operation of DLP and SLA and the differences between these VPP methods. SLA is showed to operate in a way that the controlled laser beam is focused on the build platform from above the reservoir, which is not transparent. DLP projects the light from below through a transparent reservoir bottom. However, manufacturers such as Formlabs, have SLA machines that operate in a similar manner to DLP, where a laser scanner is located below

a transparent resin reservoir. Otherwise, both of these methods have similar components, such as the sweeper, which is used to level the resin after the build platform has moved inside the reservoir. Notably the manufacturing method is different compared to for example MEX, as the build platform and manufacturing direction (the movement direction of the build platform between individual layers) is upside down.

SLA uses laser or UV light for selectively curing a layer of resin by tracing with a focused beam, after which the build platform is moved in up/down direction, and the process is repeated on top of the previous layer (Yue Ma et al., 2024; Zhu et al., 2025). Essential AM parameters for SLA include layer thickness, material choice, and irradiation exposure time. The exposure time controls the degree of solidification for the material affecting the mechanical properties of the manufactured part (Zhu et al., 2025).

DLP works similarly to SLA, but instead of using a focused beam, a whole layer of photopolymerizable resin is illuminated simultaneously with a planar light projection. The illumination is commonly performed with liquid crystal displays (LCDs) or digital micromirror devices (DMDs). LCDs operate by selectively turning single displays on or off, and a DMD consists of an array of small mirrors with on or off options to project light. The resolution of LCD or DMD is limited by the size of an individual display or mirror, determining the smallest element that is solidified on a layer. DLP has similar key AM parameters as SLA: layer thickness, material selection and exposure time. (Corrado et al., 2025; Zhu et al., 2025)

The differences in solidifying a layer between SLA and DLP are illustrated in Figure 14.

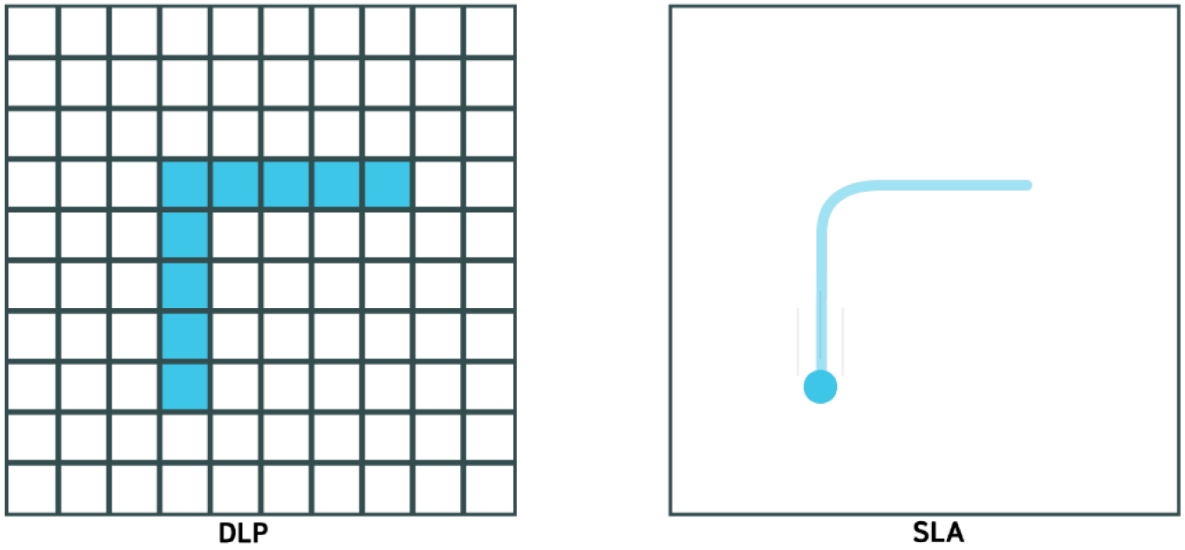


**Figure 14 Resolution difference between DLP and SLA.** "DLP" section shows how the individual pixels (LCDs or DMDs) determine the resolution of the manufactured part. In this illustration, the pixels are represented as squares, making the shape a 90-degree sharp angle. "SLA" section on the other hand has the ability to create curvature in smaller resolution, with the minimum resolution being limited by the beam diameter. Figure from Zhou et al. (2024).

Figure 14 shows how SLA offers higher resolution, as it is limited by the diameter of the beam used rather than a size or shape of an individual display or mirror, which is fixed. DLP on the other hand offers higher manufacturing speeds than SLA, as the whole layer is cured simultaneously rather than being tracked by a focused beam. For example, multiple parts can be manufactured with DLP without additional time during the AM process. With SLA however, the focused beam has to travel through the entire layer, and additional parts therefore increase the production time. SLA has capability to produce smoother curvatures and edges compared to DLP (Zhou et al., 2024; Zhu et al., 2025). The choice between SLA and DLP should therefore be made considering the resolution requirements of the intended application: manufacturing of multiple parts simultaneously and rapidly, or smoother edges and curvatures of the structure. (Zhu et al., 2025)

CLIP is a VPP method which works similarly to DLP, with the difference in z-directional, or up and down, movement. DLP moves incrementally in the z-direction, solidifying a layer at a time, but CLIP moves the platform with very minimal pauses between the solidification of layers. The weakest mechanical strength in a manufactured part is between the individual layers, as the interlayer adhesion is weaker than the bonding within a layer, similarly to MEX. Hence, as no distinct steps between layers exist when using continuous solidification, the mechanical strength is increased when using CLIP instead of using a VPP method with distinct

layers. Van Lith et al. (2016) used a CLIP system to fabricate biodegradable 20 mm long stents, with strut thickness of 150 µm. It took 70 minutes to fabricate a single 20 mm stent, with 5 µm/s platform speed. The stents could be customized and had comparable mechanical strength to commercially available metal stents. (van Lith et al., 2016)

While VPP is not commonly used with biocompatible polymers, it is compatible with some slowly biodegradable and biocompatible resins, such as polydimethylsiloxane, which is elastic and cytotoxic (Zhu et al., 2025). Other resin materials can be mixed with biocompatible materials to create bio resins. Bio resins are biocompatible, but not easily degradable, like thermoplastic polymers such as PLGA. Bio resins are designed to meet patient safety and biocompatibility regulatory standards (Zhu et al., 2025), that fulfil the safety requirements for medical device use (Khalaj et al., 2021; Yue Ma et al., 2024).

Key manufacturing parameters for VPP include curing time, curing temperature, and vat temperature, all of which are optimized based on the properties of selected resin material. VPP requires post-processing in removing the excess uncured resin by washing the manufactured part with an organic solvent such as isopropanol alcohol (Bosch et al., 2025; Dobrzańska-Danikiewicz & Bączyk, 2024). Additional post-curing in a heated UV oven is used to increase the solidification and mechanical strength of the manufactured part (Bosch et al., 2025; Zhu et al., 2025). Post-processing parameters include washing time, drying time, and post-curing temperature and time (Bosch et al., 2025).

VPP offers relatively accurate resolution when comparing to other AM methods, ranging from 10 – 100 µm (Ali et al., 2024; Corrado et al., 2025), with some novel methods reaching sub-micrometre resolutions from 0.1 – 0.7 µm (Bosch et al., 2025; Corrado et al., 2025; Nguyen & Narayan, 2017). The biomedical field uses VPP for example for manufacturing medical implants, tissue engineering scaffolds and drug delivery systems (Corrado et al., 2025; Zhu et al., 2025).

The material selection should depend on intended application. Biocompatibility, durability, stiffness, and transparency are properties that can be affected by choosing a suitable material (Zhu et al., 2025). Current research is focused on finding new biocompatible resins, suitable for use in medical applications (Dobrzańska-Danikiewicz & Bączyk, 2024). Regulations, such as European Medical Device Regulation, pose strict regulatory and safety standards for the materials used in medical devices. Even though ISO standards can give a baseline for material biocompatibility, thermal and chemical post processing required by the VPP method can impact

the biological safety of the AMed product if solvents or other residual materials are absorbed to the manufactured product (Kronenberger et al., 2025). VPP materials can withstand sterilization with high and low temperature washing and vaporized hydrogen peroxide treatment. High temperature washing may lead to cracking of the material, which should be taken into account when choosing the sterilization method for a specific material (Kronenberger et al., 2025).

VPP methods are able to create high resolution and smooth surface finished medical devices (Khalaj et al., 2021; Yue Ma et al., 2024). High precision applications, such as small and complex medical devices, benefit from the high resolution capabilities and smoother surface quality of VPP when comparing to other AM methods (van Lith et al., 2016; Zhu et al., 2025). It should be noted that shrinkage may occur during manufacturing and post processing, which can cause distortion of geometry for the printed part, lowering the dimensional accuracy (Zhu et al., 2025). Drawback of VPP methods is low mechanical strength of manufactured parts compared to other AM methods. Uneven curing can be caused by insufficient layer adhesion, which affects the structural integrity and mechanical performance of the manufactured parts (Zhu et al., 2025). Due to relatively low mechanical strength, VPP method is also not preferable for load bearing applications (Bikas et al., 2016).

A micro-precision DLP VPP machine by Boston Micro Fabrication can reach sub-millimetre resolutions as low as 2 µm (https://bmf3d.com/2µm-series-3d-printers/, cited on Dec 1st, 2025). It has been used for manufacturing stent-like structures with strut thicknesses of 150 µm and a diameter of 4.3 mm (Khalaj et al., 2021). Some VPP methods enable resolutions higher than the limitations of the optical diffraction limit. Two-photon polymerization (TPP) is an ultra-high-resolution VPP method. In a TPP process, a liquid phase photo initiator absorbs two photons, and reacts with present monomers or oligomers, causing chain growth and solidification (Liu et al., 2023). Where conventional VPP methods like SLA and DLP use for example UV photons for energy transition to cause polymerization, TPP uses two-photon absorption of near infrared light (Khalaj et al., 2021; Nguyen & Narayan, 2017). A TPP printer by Nanoscribe for example allows features of 100 nm in horizontal (xy) resolution, and stent-like structures have been manufactured using 0.1 – 5 nm layer thicknesses (Khalaj et al., 2021). Even though biomedical field benefits from ultra-high resolution and surface quality inherent for TPP methods, the method has drawbacks in higher manufacturing times, lower mechanical strength, and toxicity of usable materials. Therefore, the method has not been widely used for biomedical applications (Nguyen & Narayan, 2017).

Vakiti et al. (2025) studied the effects of part orientation and layer thickness on strain at failure and tensile strength of manufactured specimens. Parts were manufactured with orientations varying from 0 degrees to 90 degrees from the build platform and with 0.025 mm, 0.05 mm and 0.10 mm layer thicknesses. The largest tensile strength and strain at failure values were achieved with 0-degree orientation and with smallest 0.025 mm layer thickness. Tensile strength was found to increase when the tensile test specimens were manufactured in orientation that had coaxially continuous strands of material with the load direction. With increased angle between the build platform and the part, the load has to go through more individual layers of the manufactured part, creating stress concentration points in the areas where the layers connect. Interlayer bonds are weaker than the bonds within a layer, so the more the load is carried by the interlayer bonds rather than a single layer, the lower the values are for tensile strength and elongation at break. A smaller layer thickness leads to a more complete and even curing of the manufactured parts due to better penetration of the UV light of the VPP machine. (Vakiti et al., 2025)

## 4.3 Material jetting

Material jetting (MJT) method works by selectively depositing droplets of resin on the build platform and curing the layer of material with a UV light source, typically ranging from 190 to 400 nm in wavelength. After a layer has been solidified, the build platform is lowered at increments corresponding to layer thickness, and the process is repeated until the part is complete. MJT allows for use of multiple materials for a single part during the same manufacturing process, as multiple nozzles can be used simultaneously. (Ali et al., 2024; Gülcan et al., 2021; Khalaj et al., 2021)

Gel-like support structures are required around overhangs of the 3D part, as MJT uses uncured resin as material, which is not self-supportive. Support structures can be removed in multiple ways: a solution bath, by heating, or with a high-pressure water jet (Gülcan et al., 2021). After the removal of support structures, the parts are ready to be used without additional post-processing (Ali et al., 2024; Dobrzańska-Danikiewicz & Bączyk, 2024).

MJT technology has advantages in thin layer thicknesses as low as 16 µm, which provides a surface with little or no noticeable stair-step structures between individual layers, resulting in a smooth surface finish (Dobrzańska-Danikiewicz & Bączyk, 2024; Gülcan et al., 2021). MJT also enables small structures, with printing resolutions as good as 15 µm in xy-direction (Dobrzańska-Danikiewicz & Bączyk, 2024). The method has relatively little deviation in

dimensional accuracy of manufactured parts, but it is not well suited for fabricating small holes (< 1 mm in diameter) in the manufactured parts. Another downside is the high costs of MJT machinery when comparing to for example MEX or VPP machinery (Gülcan et al., 2021).

MJT is currently used in rapid prototyping and tool fabrication with high resolution, for example in injection moulding for mould and insert fabrication (Gülcan et al., 2021). As MJT is capable of multi-material and multi-colour 3D-printing, the biomedical field can use it for example for hand prostheses, surgical training models, and other multi-colour or -material models (Ali et al., 2024).

Moore et al. (2016) used Poly-Jet technology with 50 µm droplet size for the photosensitive polymer, which was solidified immediately after deposition. They fabricated stents with outer diameters ranging from 4 mm to 10 mm, with intricate wall structure, and a strut thickness of 400 µm. The stents are shown in Figure 15 a-b.

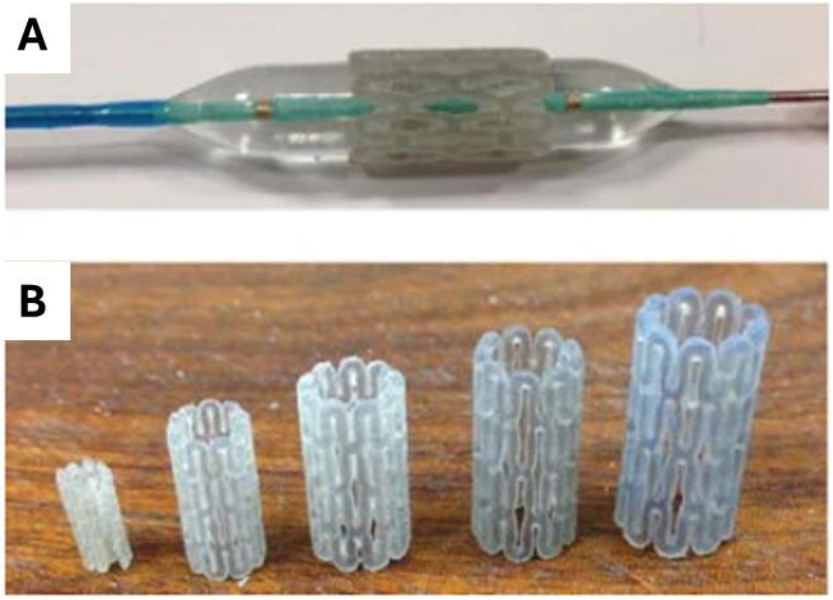


**Figure 15 Stents fabricated by Moore et al. (2016) with MJT AM method.** The smallest model on the left side of section B has an outer diameter of 4 mm, and the largest on the right side has a diameter of 10 mm. All of the stents have a strut thickness of 400 µm. Section A of the figure shows a stent inserted onto a balloon catheter. Figure from Moore et al. (2016).

Figure 15 a-b shows the stents fabricated with MJT method by Moore et al. (2016). Even though the manufacturing process was successful to the point of receiving complete products from the machine, all the stents manufactured failed mechanically during expansion testing on a balloon catheter, seen in Figure 15a. The failures occurred due to delamination, or separation of subsequent layers, caused by insufficient bonding between the individual layers of the

manufactured stents. It was noted that the machine was not well suitable for fabricating small scale stent prototypes, but that a smooth surface finish was achieved without post-processing. (Moore et al., 2016)

The material used by Moore et al. (2016) was not a biocompatible resin. Starsys, which is the manufacturer of the MJT machine used by Moore et al., does provide biocompatible materials intended for applications that may require prolonged skin contact (30 days or more) or short-term mucous membrane contact (24 hours or less) (*Biocompatible Materials | Stratasys Support Center*). These are not however suitable for intravascular use.

## 4.4 Binder jetting

A typical binder jetting (BJT) process is illustrated in Figure 16.

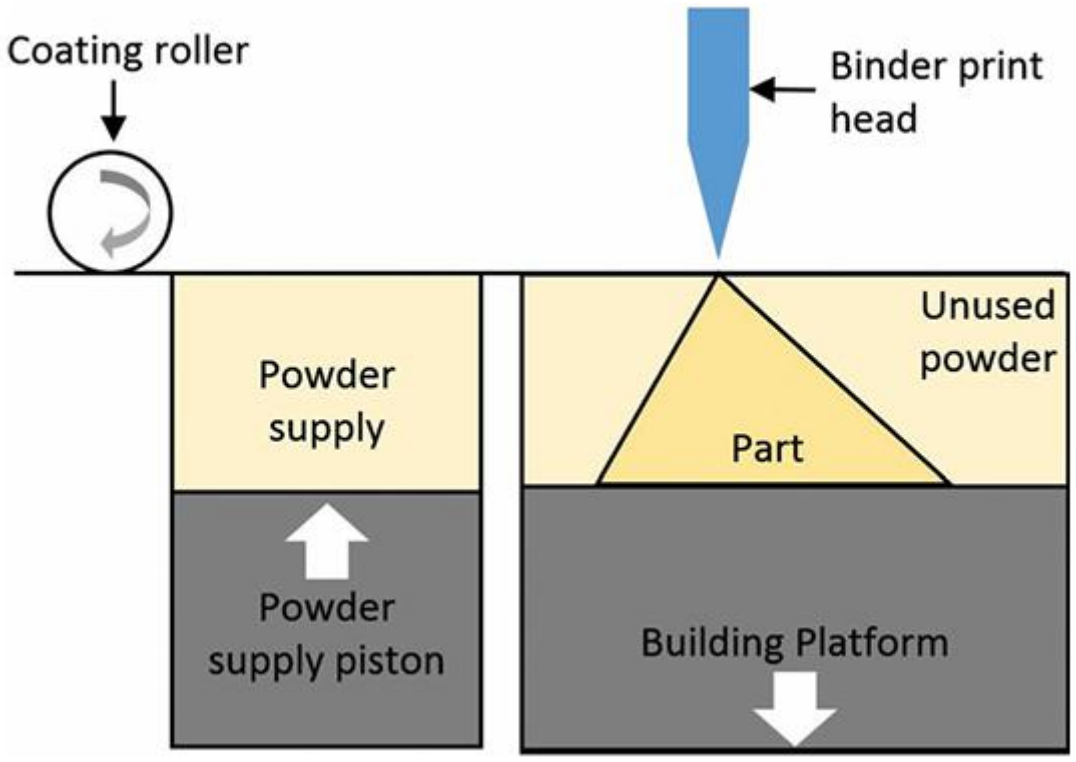


**Figure 16 Operation principles of a BJT machine.** An even layer of powder raw material is supplied with a roller on top of the building platform. Liquid binder material is selectively applied on top of the layer from the blue binder print head to solidify the layer of the part. The build platform is lowered, and the process is repeated. Figure from Bikas et al. (2016).

As seen in Figure 16, the BJT process works by dispensing polymer powder from a reservoir to the building platform. In Figure 16, the supply is completed by pushing the powder supply upwards with the powder supply piston and spread evenly on the building platform with the

coating roller (Farazin et al., 2025). Low-viscosity liquid binder solution is selectively deposited from the binder print head, shown in Figure 16, as droplets to the evenly spread powder layer, and it acts as an adhesive between the individual layers of the part (Khalaj et al., 2021). After the layer is complete, the building platform is lowered, and the process is repeated until the geometry of the part is completed (Ali et al., 2024; Farazin et al., 2025). Post processing typically includes removal of excess powder, and as the parts fabricated with BJT are porous, they are exposed to a liquid, such as epoxy resin, to increase mechanical strength and improve surface smoothness (Khalaj et al., 2021). Different manufacturing parameters include layer thickness, drying time, spreading speed of the powder material, powder size, and powder size distribution (Ali et al., 2024).

BJT offers a wide range of usable materials and high manufacturing speeds, at the cost of increased post-processing requirements through thermally removing the binder out of the processed product. As the manufacturing and post-processing require heat, shrinkage of the parts is also inherent to the BJT AM method. (Dobrzańska-Danikiewicz & Bączyk, 2024)

BJT can manufacture parts made from biocompatible and biodegradable polymer composite materials, such as PCL mixed with biphasic calcium phosphate (BCP). The mixture is biocompatible and biodegrades inside the human body. It can be used for example to create hard tissue regenerative temporary scaffolds. This kind of composite materials exhibit good biosafety, as well as mechanical strength. (Ahn et al., 2021) BJT does not provide good xy-resolution or surface quality compared to other polymer AM methods, as can be seen in Figure 17, showing test specimen manufactured by Ahn et al. (2021).

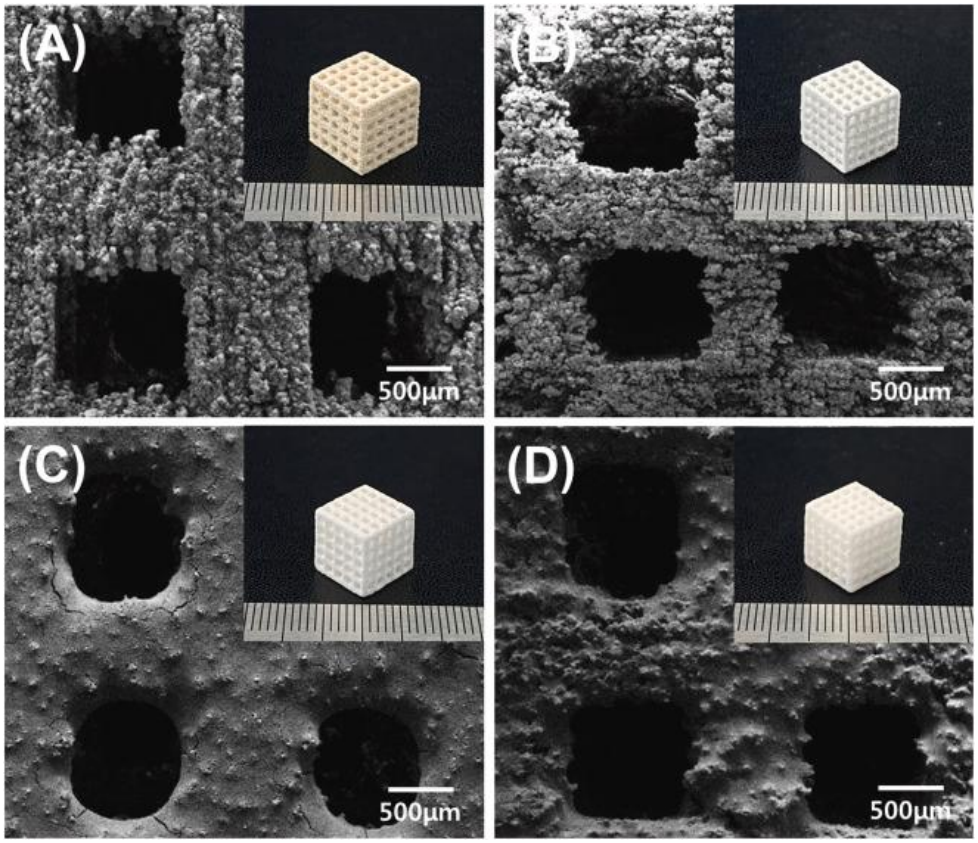


**Figure 17 Surface quality and resolution visualization for BJT parts.** The figure shows different materials that were used to manufacture test specimen with a BJT method. Figure from Ahn et al. (2021).

As seen in Figure 17 a-d, specimen fabricated with BJT have rough surface quality even in the 500 µm reference scale. The dimensional accuracy is also poor, especially in Figure 17a and Figure 17b.

BJT is currently used for example for rapid prototyping and electro-chemical applications. (Farazin et al., 2025). The method is not widely used in biomedical applications, but some custom implants and porous structures, such as bone scaffolds have been created with BJT (Ahn et al., 2021). Figure 18 shows bone scaffolds and femoral interference screws fabricated with BJT.

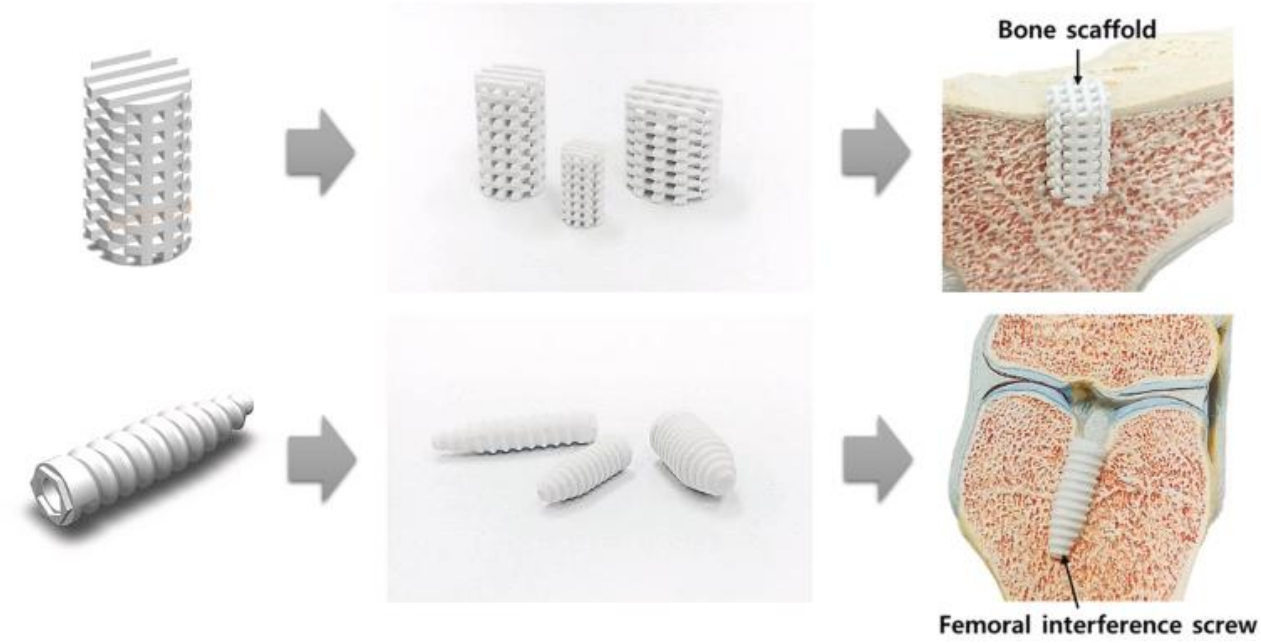


**Figure 18 Bone scaffold and Femoral interference screw, manufacturable with BJT.** The Bone scaffold and Femoral interference represent biomedical applications, to which BJT methods can be applied to. Figure from Ahn et al. (2021).

The bone scaffolds and femoral interference screws seen in Figure 18 have relatively large dimensions and detail sizes when comparing to vascular stents, which have strut thicknesses as low as 200 µm. Even though BJT can be used to manufacture larger medical devices, the resolution capability is not sufficient for small strut thicknesses.

Bone scaffolds on the other hand benefit from the inherent porousness of the structure created with BJT, as it allows for blood or other bodily fluids to flow through the structure. This enhances tissue regeneration and tissue growth, while simultaneously providing sufficient mechanical support for bone regeneration. Since 2015, BJT has been viable for use in the pharmaceutical industry as FDA approved the first medicine tablet manufactured with a BJT method (Farazin et al., 2025).

## 4.5 Powder bed fusion

A common PBF work cycle is illustrated in Figure 19.

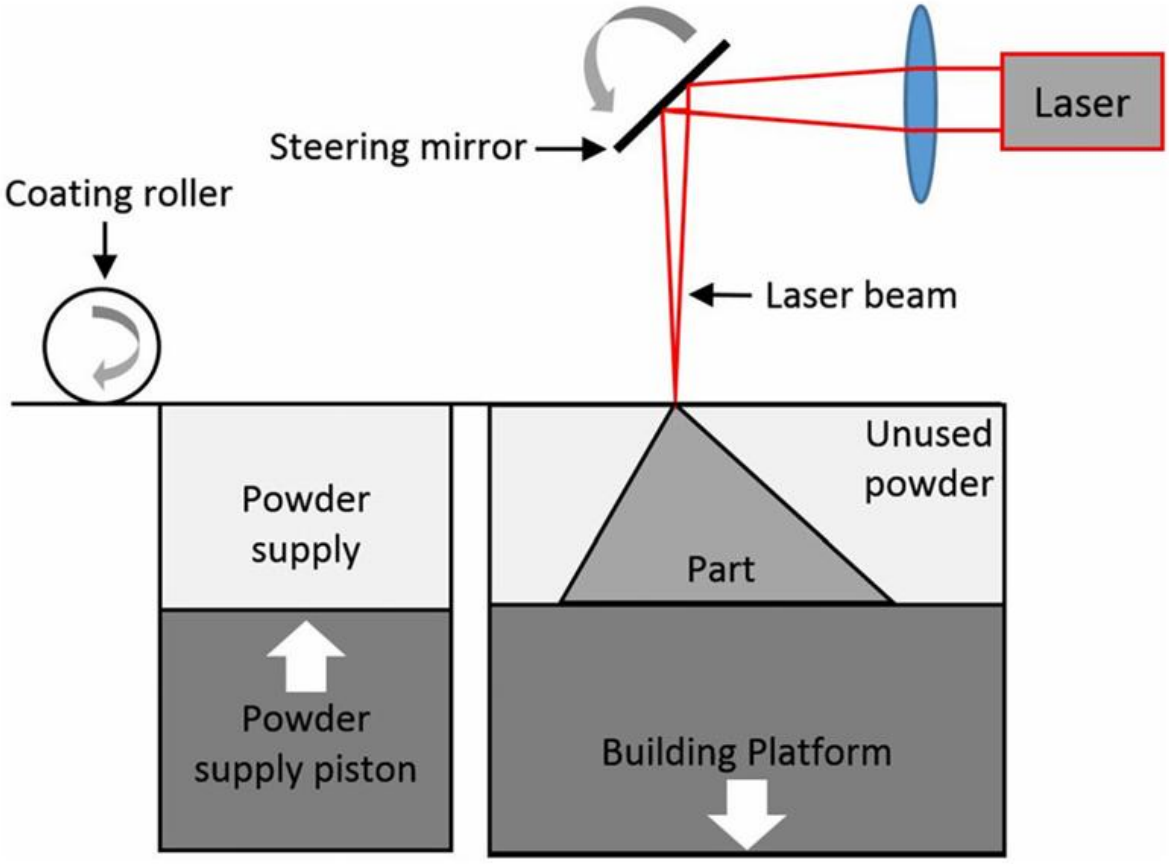


**Figure 19 Operating principles of a PBF machine.** Similarly to a BJT machine, the powder is supplied as an even layer on top of the build platform with the powder supply piston. An energy beam, in this case laser, is applied to a focusing scanner (steering mirror). The beam is traced on the build platform to selectively melt the powder. After melting, the powder solidifies to form a layer of the manufactured part. The building platform is lowered and process is repeated until the part is completed. Figure from Bikas et al. (2016).

As seen in Figure 19, the PBF work cycle is similar to BJT. It begins by supplying fine powdered material from the powder supply evenly on the build platform with the coating roller. The powder material is selectively melted and solidified by scanning the layer geometry with a focused laser (as seen in Figure 19) or electron beam (Bikas et al., 2016; Farazin et al., 2025; Flege et al., 2013). The molten material then cools down and forms a solid layer of the manufactured part. After the layer is completed, the build platform is lowered, a new layer of powder is added, and the process is repeated until the part is completed (Bikas et al., 2016; Farazin et al., 2025). It should be noted that the build platform is full of powder material during

the manufacturing process. Some heat conduction is present near the melted area, which can cause dimensional inaccuracies and surface roughness when semi-molten particles attach to the solidifying layer. There are also benefits, as the powder acts as support during manufacturing, so the requirements for additional support structures are reduced. The whole build volume can also be used for manufacturing multiple parts simultaneously, with no required contact with the base of the build platform.

PBF requires post processing steps for removal of non-molten particles, removal of support structures, and heat treatments for enhancing the mechanical properties of the part (Zhu et al., 2025). Heat treatment can be done for example by annealing, which is a process of heating the manufactured part above the glass transition temperature, holding the annealing temperature for a set time, and allowing the part to cool down. This allows the polymer chains to reorganize into a more crystallized structure, which leads to improved mechanical properties such as tensile strength and elongation at break, and also makes the mechanical performance more isotropic as interlayer fusion is increased (Magri et al., 2022).

PBF has two different methods for melting the powder: electron beam PBF (PBF-EB) and laser beam PBF (PBF-LB). PBF-LB requires the use of a protective gas, whereas PBF-EB requires a vacuum state during printing. PBF-EB is generally much more expensive due to required vacuum pumps, electron guns and high-voltage generators but does not require protective gases. PBF-EB can be used to create high resolution parts (Dobrzańska-Danikiewicz & Bączyk, 2024). However, PBF-EB can only be used on powder materials that conduct electricity, and therefore it is not suitable for producing polymer components. Another common division with PBF methods is based on the feedstock material used. For example, selective laser sintering is a commercial name for laser beam PBF of polymers (PBF-LB/P), and selective laser melting is correspondingly used with laser beam PBF of metals (PBF-LB/M) (Zhu et al., 2025). The commercial names can be confusing, and therefore only the standardized terms and abbreviations should be used, such as PBF-LB/P or PBF-LB/M. As this thesis however only focuses on polymer AM methods, and electron beam cannot be used for melting polymer powder materials, PBF is used to abbreviate (laser) powder bed fusion of polymers.

PBF is compatible with various biocompatible and biodegradable polymers used in biomedical applications (Flege et al., 2013; Zhu et al., 2025). The most used are PLA and PCL. The powder materials should be handled and recycled properly to maintain good results in consistency and surface quality of manufactured parts (Zhu et al., 2025). Essential manufacturing parameters

for PBF include the powder material selection, power and type of beam used for melting, scanning speed of the beam, power of the beam, track distance and overlap, and layer thickness (Flege et al., 2013; Zhu et al., 2025). An illustration of different manufacturing parameters can be seen in Figure 20.

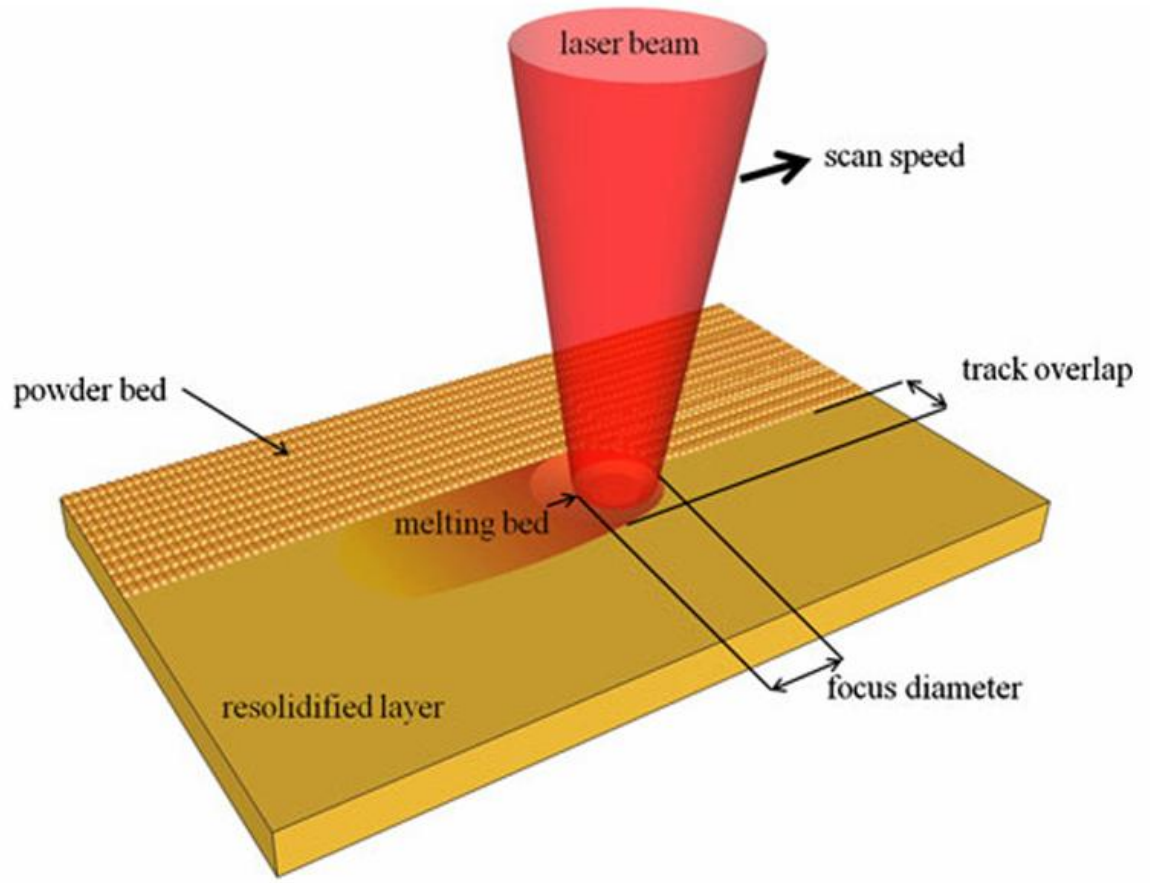


**Figure 20 Illustration of PBF-LB manufacturing parameters.** Scan speed, focus diameter and laser power affect the thermal energy that is applied to the powder material during the PBF manufacturing process. Figure from Flege et al. (2013).

Figure 20 illustrates the different PBF manufacturing parameters. Size of the melt pool in the melting bed is affected by the power of the laser beam, beam diameter, scan speed, number of repeated scans, and track overlap. The thickness of the manufactured structure is dependent on the melt bed size, as a larger melt bed results in a wider track (Flege et al., 2013). The total amount of exposure time the powder material receives from the beam determined by scanning speed, power of the laser, and number of scans, affects the melting and solidification behaviour of the powder material. Scanning speed of the beam also determines the amount of time the manufacturing process takes. These parameters need to be optimized to achieve desired surface

quality, integrity of structure, and dimensional accuracy of the manufactured parts (Zhu et al., 2025).

Material properties like powder particle size and polymer composition also affect the material behaviour during beam interaction. Thermal properties of the polymer powder affect energy absorption and dissipation, which may lead to variations of mechanical properties in parts manufactured with PBF methods. (Zhu et al., 2025)

PBF offers good resolution, design flexibility, and wide range of usable materials (Zhu et al., 2025). Formlabs Fuse 1+ 30 W PBF machine for example offers a layer thickness capability of 110 µm, which corresponds to z-axis resolution, and a focused laser spot size of 247 µm, which affects the planar x-y resolution capability. (https://formlabs.com/eu/3d-printers/fuse-1/, cited on 14$^{th}$ October, 2025).

Flege et al. (2013) manufactured polymeric coronary stents with PBF method. Stent prototypes were manufactured from biocompatible and biodegradable PLLA and PCL powder materials. Manufactured parts from both of the materials could withstand gamma sterilization. The biological properties of the polymers did not alter during the PBF manufacturing process. These factors make the PBF method seemingly suitable for medical device manufacturing when using acceptable materials. Stent prototypes with 3 mm outer diameter and strut thickness of 180-200 µm were manufactured, shown in Figure 21.

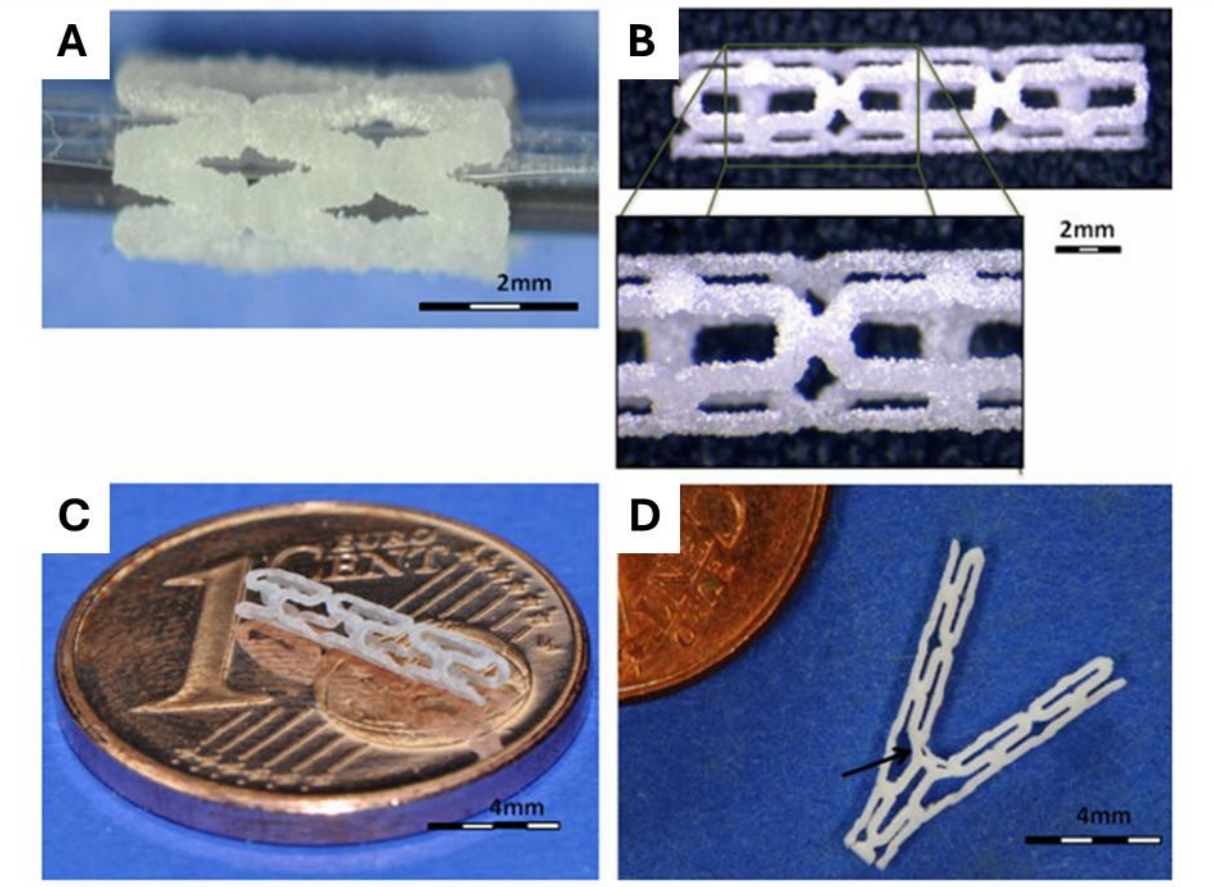


**Figure 21 Stent prototypes manufactured by Flege et al. (2013).** Section A shows a prototype with thicker strut thickness made from PCL, inserted on a balloon catheter. Sections B and C show prototypes made from PLLA, with longer and rounder wall structures and thinner strut thicknesses. Section D shows a different "Y-structured" stent. Figure taken and modified from (Flege et al., 2013).

PBF manufacturing used left a rough, uneven surface finish, as can be seen in Figure 21a and 21b. Thickness of struts were affected by three factors: laser beam diameter, laser power, and the number of repeated scans of the powder layer. Thickness was lowered by decreasing the beam diameter and increasing the number of repeated scans. (Flege et al., 2013)

Flege et al. (2013) used a combination of spray and dip coating to counter the surface roughness and ultimately leave an even and smooth surface finish on the inside and the outside structures of the tubular stent prototypes. Dip coating was performed in a solution of 1 % chloroform PLLA solution. Pressure blowing was done after the dipping to remove excess chloroform from the surface. Finally, the parts were dried in a 40-degree Celcius oven for 16 hours after coating to remove the rest of the chloroform. Spray coating was done with the same 1% chloroform solution, and similar drying was performed afterwards. Drying was performed both in the between, and at the end, when combining both dip and spray coating. Surface roughness with different treatment combinations are seen in Figure 22.

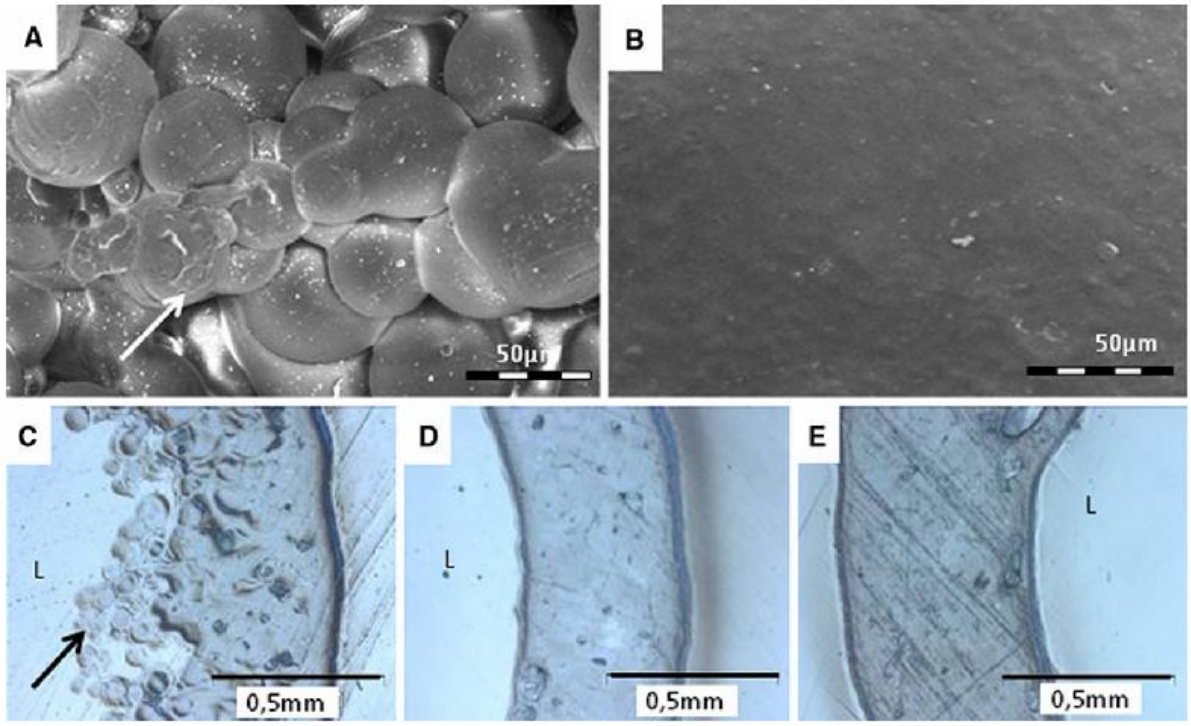


**Figure 22 Surface finish before coating and after coating.** The images were taken with photomicrograph. (A) illustrates the reason for a rough surface finish inherent to PBF AM method due to individual polymer powder particles adhering to the surface of the part during manufacturing. (B) shows the surface finish after a combined dip and spray coating. (C) shows the surface finish of a tubular stent after spray coating, (D) shows the surface after dip coating and (E) shows the finish with a combination of dip and spray coating. L in the images refers to the inner (lumen) side of the tubular stent. Figure taken from Flege et al. (2013).

Figure 22 shows the surface roughness before and after coating for the stent prototypes manufactured with PBF. Figure 20A illustrates why the surface roughness is inherent to the AM method, as unmolten polymer powder particles have adhered to the surface of the part during manufacturing. Figure 20B shows the effects of coating after the part has been manufactured, resulting in a smooth surface. Figure 20C shows how the spray coating only addresses the outer surface of the post-processed stent prototype, leaving the inner surface of the tube very uneven. The inner surface also receives a smoother surface when dip coating is used, as seen in Figure 20D. The visually best result was achieved by combining both of the used coating methods, as seen in Figure 20E.

## 4.6 Summary table

Table 1 summarizes the findings of the literature review. The comparison criteria are based on the requirements for BRSs.

Table 1: Summary of different polymer AM methods with selected criteria.

| **Comparison criteria** | **MEX** | **VPP** | **MJT** | **BJT** | **PBF** |
|---|---|---|---|---|---|
| **Smallest achievable xy resolution** | 200 – 600 µm | 10 – 100 µm, (TPP < 1 µm) | 15 – 50 µm | 100 – 300 µm | 150 – 300 µm |
| **Dimensional accuracy** | poor / moderate | excellent | good | poor (shrinkage) | good |
| **Surface quality** | poor | excellent | excellent | poor | poor without post-processing |
| **Availability of biocompatible materials** | good | limited | limited | moderate | good |
| **Availability of biodegradable materials** | good | limited | practically none | moderate | good |
| **Mechanical strength** | poor / moderate | poor / moderate | moderate | moderate/good | good |
| **Anisotropic mechanical properties** | high | moderate | moderate/high | moderate/low | low |
| **Thin walled (<200 µm) structure manufacturing** | not realistic | possible | poor (delamination) | not realistic | possible |
| **Post-processing requirements** | low / moderate | high | low | high | moderate |

# 5 Aim and purpose of experimental part

The experimental part creates a decision-making framework for contextually selecting a suitable polymer AM method based on the intended use case, as there is no clear guideline for selecting a polymer AM method from all the available methods for fabricating medical devices. An emphasis is placed on the requirements of the medical device prototype, as regulations are key factors for medical devices.

The decision-making model consists of two parts. A weighted base score matrix and a decision-making tree. The weighted base score matrix is based on the findings of the literature review presented in Table 1, with weight factors calculated for each comparison criteria by the Analytical Hierarchy Process (AHP), a multi-criteria decision-making method method developed by Thomas Saaty in 1980 (as cited by Mançanares et al., 2015). The AHP method works well when comparing options through multiple differentiating comparison criteria, making it a suitable method for comparing the five polymer AM methods with the nine comparison criteria presented in Table 1. The AHP method has been used for determining suitability of AM methods, providing a transparent method for prioritizing comparison criteria according to the use case (Mançanares et al., 2015). The decision-making tree consists of a set of questions, which are based on requirements of BRSs. The questions guide the decision-making logically by ruling out unsuitable polymer AM methods by the hard constraints in the questions.

Together the AHP method for multiple criteria decision-making, and the decision-making tree, address the challenge of determining the most suitable polymer AM method and provide an overview of the decision-making process based on the use case (context) of the prototypes.

# 6 Experimental setup

## 6.1 Prototyping scenarios

The framework is context-dependant, meaning that the outcome of the most suitable polymer AM method may vary based on the use case of the fabricated prototype. The most suitable polymer AM method cannot be determined without defining the intended purpose of the medical device prototype. For this reason, two prototyping scenarios for the medical device prototype are defined:

1. Implantable prototype intended for *in vivo* (in contact with living tissue) use or mechanical testing in physiologically realistic environmental conditions.

2. Geometry-only prototypes intended for determining functionality of the design of the prototype without implantation.

In scenario 1., the prototype is intended for implantation or mechanical testing closely resembling *in vivo* stress conditions, such as balloon expansion of a vascular stent. Strict material biocompatibility, biodegradability, and mechanical performance requirements are needed with this scenario. In scenario 2., the prototype is used for evaluating the functionality of the geometry. The mechanical loading is limited to handling and visual inspection, and biodegradability or biocompatibility material properties are non-essential. If the geometry can be studied in a larger scale, for example between 2:1 to 5:1, the resolution capability limitations of different polymer AM methods become less critical for manufacturing thin-walled medical device prototypes.

## 6.2 Base score matrix

A base score matrix is created so that the weight factors calculated with the AHP method can be implemented to the literature review findings to give final scores for each AM method, based on which the most suitable polymer AM method can be determined for each prototyping scenario.

The base score matrix gives quantifiable values for the literature review findings presented in Table 1. The matrix gives a relative score for each polymer AM method in each comparison criteria. The comparison criteria are smallest achievable xy-resolution, dimensional accuracy, surface quality, availability of biocompatible and biodegradable materials, level of anisotropic

mechanical properties, thin-walled structure manufacturing capability, and post-processing requirements. The comparison criteria were selected to cover the key manufacturing, material property, and quality factors for fabricating a prototype according to the device description presented in chapter 1.3. As the device description resembles a BRS, AM methods can be differentiated by their capability in producing BRS-like devices.

Xy-resolution, dimensional accuracy, and capability of producing thin-walled structures are important as the device is thin-walled with small features and strut thicknesses around 200 µm. Surface quality is an important factor for a BRS, and the device described in chapter 1.3 resembles a BRS. Additionally, the surface quality affects the dimensional accuracy when the device is small. Biocompatibility and biodegradability are crucial when manufacturing a medical device that is intended for *in vivo* use. Mechanical strength and anisotropy of mechanical properties require consideration when the device is subjected to directional loads, such as during balloon expansion of stents shown in Figures 7a-c and 15a. Post processing requirements should be considered especially if the time taken for manufacturing a single device prototype is an issue, for example during a rapid design iteration phase, where changes to the design are done and tested in an iterative loop over a short period of time.

## 6.3 Analytical Hierarchy Process for weight factor calculation

Weight factors are calculated for each comparison criterion, and the weight factors are context-dependant according to the requirements of the prototyping scenario. The weight factors are calculated by the AHP method, and a weighted sum of scores is calculated for all polymer AM methods by multiplying the base score matrix with the corresponding weight factors for each comparison criteria and summing the scores for each AM method.

The weight factors are calculated by comparing each criterion against all the other criteria, by giving a differentiating factor of 1 to 9 to the more important criterion. The rationale for the weight factors are presented in Table 2.

Table 2: AHP importance factor definition, derived from Saaty, 2008.

| Intensity of importance | Definition |
|---|---|
| 1 | Equal |
| 2 | Slight |
| 3 | Moderate |
| 4 | Moderate plus |
| 5 | Strong |
| 6 | Strong plus |
| 7 | Demonstrated importance |
| 8 | Very, very strong |
| 9 | Extreme importance |

The intensity of importance in Table 2 determines how much more important a comparison criterion is compared to another criterion. For example, by giving availability of biocompatible materials an intensity of importance of 5 over post processing requirements, it means that the availability of biocompatible materials is strongly more important than post processing requirements.

By giving the comparison criteria incremental values in comparison to each other, the AHP method is based on mathematics and therefore transparent and repeatable. The AHP process is described in detail by Saaty (2008), and an example of the weight factor calculation is provided in chapter 7.3. The pairwise comparisons are presented in a pairwise comparison matrix, which has a dimension determined by the amount of comparison criteria. In the experimental part, the dimension is nine, as there are nine comparison criteria considered for the prototyping scenarios. In the case of biocompatible materials having an intensity of importance value of 5 against post processing requirements, on the row “i” the biocompatible materials would have a value of 5 in the column “j” where the post processing requirements is, and on the row of post processing requirements, the value would be 1/5 on the column where the biocompatible materials is. This comparison is executed between all the comparison criteria, and the pairwise comparison matrix is filled with the determined values given by the person(s) comparing the criteria.

## 6.4 Consistency Ratio

Logical coherence of the weight factor calculations is verified with a consistency ratio (CR) calculation. The CR calculation procedure is described by Taherdoost, (2017), and an example of the CR calculation is provided in chapter 7.4. The CR simply checks the logic, that if comparison criterion A is more important than comparison criterion B, and B is more important than C, it should follow that A is more important than C as well.

Weighted sum vectors ($d_i$) are calculated by matrix operations demonstrated in chapter 7.4. The weighted sum vectors are divided by the corresponding weight factors.

The largest eigenvalue $\lambda_{max}$ is then calculated as an average with the equation:

$$\lambda_{max} = Avg.(^{d_i}/_{w_i}) \tag{1}$$

And the consistency index (CI) is calculated with the equation:

$$CI = \frac{\lambda_{max} - n}{n - 1} \tag{2}$$

where n represents the number of comparison criteria and the dimension of the pairwise comparison matrix, which is 9 in the experimental part.

Finally, the CR is calculated with the consistency index and random index (RI) with the equation:

$$CR = {}^{CI}/_{RI}\,. \tag{3}$$

Where the RI value is selected from Table 3, according to the dimension of the pairwise comparison matrix. A CR value lower than 0.10 is acceptable, otherwise there are notable inconsistencies in the pairwise comparison matrix, and the comparisons have to be re-assessed.

Table 3. RI values according to the pairwise comparison matrix dimension, from (Taherdoost, 2017).

| Dimension | RI value |
|---|---|
| 1 | 0 |
| 2 | 0 |
| 3 | 0.58 |
| 4 | 0.89 |
| 5 | 1.12 |
| 6 | 1.24 |
| 7 | 1.33 |
| 8 | 1.40 |
| 9 | 1.45 |
| 10 | 1.49 |

## 6.5 Decision-making tree model

The decision-making tree model guides the user through five sequent questions and sub-questions, which narrow down the selection of suitable polymer AM methods before the weighted comparison matrix derived through the AHP process is used. The tree works as a filter based on hard constraints, which remove unsuitable polymer AM methods from consideration. The remaining AM methods can be assessed through the ranking based on the AHP method.

Question 1: Is the prototype intended for implantation or *in vivo* use / testing?

- Yes: Scenario 1 weight factors are applied.
- No: Scenario 2 weight factors are applied.

Question 2: Will the medical device be used or tested in contact with living tissue?

- No: Any method is suitable, as there are no additional material constraints.
- Yes: Only methods with available biocompatible material selections are viable. MJT is eliminated, VPP remains viable only with certified biocompatible resins.

Question 3: Does the medical device include details smaller than 200 µm?

- No: Any method is still suitable.
- Yes: Question 3.1: Can the device be tested or used in larger scales (e.g. 2:1 to 5:1)?
    - Yes: All methods remain suitable as scaling removes detail resolution limitations.
    - No: MEX eliminated due to nozzle diameter limitations, BJT eliminated due to post-processing shrinkage. It should be noted that PBF operates at the boundary of this threshold.

Question 4: Will the medical device be subjected to a load?

- No: all remaining methods viable.
- Yes: Question 4.1: Will the load be uniform or directional?
    - Uniform: Anisotropic mechanical properties are important. PBF and BJT strongest in this regard, while MEX and MJT have higher anisotropy in mechanical properties.
    - Directional: PBF has the best overall mechanical strength. BJT is near PBF and comes second. Other methods can be used but manufacturing orientation should be taken into account to counter problems with delamination or otherwise weaker directions depending on the printing direction.

Question 5: Does surface quality affect the functionality of the medical device prototype?

- No: All remaining methods are viable.
- Yes: Question 5.1: Does post-processing affect the usability of the medical device prototype?
    - No: All methods viable, but surface quality improving post-processing requirements expected for PBF, MEX and BJT.
    - Yes: Methods with good as-manufactured surface quality are preferred (MJT, VPP).

# 7 Experimental procedure

## 7.1 Base score matrix rationale

Each polymer AM methods receive scores from 1 (the best) to 5 (the worst) for each comparison criterion based on qualitative findings summarized in Table 1. In cases where several AM methods have similar properties on a single comparison criterion, they share a score.

The scoring rationale for the criteria is as follows:

For smallest achievable xy-resolution, VPP methods rank highest as they can reach resolutions of 10 – 100 µm (Ali et al., 2024; Corrado et al., 2025), and methods such as TPP can reach sub-micrometre resolutions (Liu et al., 2023). VPP is followed by MJT at 15 – 50 µm resolution capability (Dobrzańska-Danikiewicz & Bączyk, 2024). PBF and BJT are in 100 – 300 µm range (Flege et al., 2013; Khalaj et al., 2021), and MEX places last, limited to 200 – 600 µm resolution due to nozzle diameter restrictions (Corrado et al., 2025).

For dimensional accuracy, VPP is again ranked highest due to precise light-based curing (Zhu et al., 2025). MJT comes second, as good dimensional accuracy can be achieved with good droplet control (Gülcan et al., 2021). PBF can achieve good accuracy, but some thermal distortion is present (Zhu et al., 2025). MEX comes second to last, suffering from effects such as warping and nozzle-related inaccuracies (Bouzaglou et al., 2023; Spina, 2025). BJT falls shortest in this category, due to shrinkage during post-processing heat treatment required for binder removal (Dobrzańska-Danikiewicz & Bączyk, 2024).

For as-manufactured surface quality, VPP and MJT share the best score. VPP methods achieve smooth surfaces through light-based curing (van Lith et al., 2016; Zhu et al., 2025), and MJT can produce smooth surfaces due to low, down to 16 µm, layer thicknesses, minimizing the stair-step structures in the manufactured parts (Gülcan et al., 2021). PBF and BJT produce rough surfaces due to powder adhesion, and BJT additionally has higher porosity of the manufactured structure (Flege et al., 2013; Khalaj et al., 2021). MEX receives the worst score in surface quality due to notable stair-step structures (Farazin et al., 2025; Singh et al., 2025).

For availability of biocompatible materials, MEX has the widest selection of FDA-approved usable biocompatible thermoplastics, such as PLA, PCL, and PLGA (Bouzaglou et al., 2023; Kulker et al., 2025; Zhu et al., 2025), followed closely by PBF with powder materials such as PLA, PLLA, and PCL (Flege et al., 2013; Zhu et al., 2025). BJT has demonstrated compatibility

with some biocompatible materials, such as PCL infiltrated into BCP scaffolds (Ahn et al., 2021). VPP can use biocompatible resins, but the selection is smaller than for thermoplastic material using methods (Zhu et al., 2025). MJT does not have biocompatible materials that could be used in intravascular implant applications, but they can be used for short-term mucous tissue contact or longer-term skin contact requiring applications. It still places last in this criterion category.

For availability of biodegradable materials, MEX and PBF share the best score as both of them can use similar biodegradable thermoplastic materials such as PLA, PCL and PLLA, which degrade through hydrolysis (Flege et al., 2013; Guerra et al., 2017; Park et al., 2015). BJT can use some biodegradable materials (Ahn et al., 2021). VPP has some resin materials that biodegrade within many years (Zhu et al., 2025). MJT effectively has no biodegradable material options.

For mechanical strength, PBF produces the strongest parts, and the mechanical strength can be further improved through post-processing, for example annealing (Flege et al., 2013; Magri et al., 2022). BJT offers mechanical strength through post-processing, and by using ceramic materials together with polymers (Ahn et al., 2021; Khalaj et al., 2021). MJT produces parts with moderate strength, but delamination has been found to occur for stent-like devices (Moore et al., 2016). MEX and VPP share the lowest score due to poorest interlayer fusion which causes mechanical weaknesses (Bouzaglou et al., 2023; Zhu et al., 2025).

For anisotropy of mechanical properties, PBF produces the best parts, with the ability to produce parts with nearly isotropic mechanical properties, especially after annealing (Magri et al., 2022). BJT comes second through post-processing and even spreading of materials in the polymer / ceramics matrix (Ahn et al., 2021). VPP shows moderate anisotropy and MJT shows moderate to high anisotropy, for example with delamination tendencies (Moore et al., 2016). MEX exhibits high anisotropy, due to weak interlayer bonds (Bouzaglou et al., 2023; Spina, 2025).

For thin-walled structure manufacturing, VPP has demonstrated best capability of manufacturing medical devices, such as stent-like structures with strut thicknesses of 150 µm (Khalaj et al., 2021; van Lith et al., 2016). PBF can achieve 180 – 200 µm strut thicknesses, which are right at the limit of 200 µm (Flege et al., 2013). MJT is able to produce wall thicknesses of roughly 400 µm (Moore et al., 2016). MEX and BJT are the worst in this category, with neither being close to producing struts of 200 µm. MEX has limitations in nozzle

diameter and solidification behaviour of the feedstock material (Spina, 2025; Zhu et al., 2025), and BJT suffers from high dimensional inaccuracies, making small strut thicknesses impossible to produce (Dobrzańska-Danikiewicz & Bączyk, 2024).

For post-processing requirements, MJT achieves the best score, with little to no need for post-processing stages (Gülcan et al., 2021). MEX requires moderate manual support structure removal. PBF requires powder removal, and perhaps surface coating or annealing to achieve sufficient mechanical strength and surface quality (Flege et al., 2013; Magri et al., 2022). VPP parts go through removal of uncured resin with organic solvents such as IPA, and post-curing (Bosch et al., 2025; Zhu et al., 2025). BJT requires multiple steps: binder removal, infiltration, and necessary heat treatments (Dobrzańska-Danikiewicz & Bączyk, 2024).

## 7.2 AHP pairwise criteria comparisons

The pairwise comparisons in this thesis were performed by the author, based on the known requirements of the medical device described in chapter 1.3, the findings of the literature review in chapters 2-4, and the setting of the prototyping scenarios described in chapter 6.1. Each pairwise comparison was done according to the AHP method, with intensity factors presented in Table 2.

Pairwise comparisons in scenario 1 highlight the importance of material biocompatibility and biodegradability, as without these prerequisites the medical device prototypes cannot be used in the intended environment. Thin-walled manufacturing is also essential together with sufficient xy-resolution to produce struts with thicknesses near or under 200 µm. Mechanical strength is required especially during balloon expansion. Surface quality (as-manufactured) and post-processing requirements are less important as surface coating or other post-processing is a standard in many stent-like medical devices. The pairwise comparison matrix for scenario 1 is presented in Table 6 in appendix 1.

The pairwise comparisons for scenario 2 reflect the need for rapid iteration capability through lower post-processing requirements, including good as-manufactured surface quality. For visual inspection, the part should represent the geometry accurately, but as it is not actually implanted or used in real environment, the prototype can be manufactured in larger scales. The xy-resolution is therefore less important, but the polymer AM method still must be able to produce thin-walled structures. Biocompatibility and biodegradability are not essential as the

prototype is not in contact with living tissue. The pairwise comparison matrix for scenario 2 is presented in Table 10 in appendix 2.

## 7.3 AHP method workflow

After the pairwise comparisons are completed, the AHP method workflow proceeds as follows:

1. Comparison criteria are organized into pairwise comparison matrices, where elements $a_{ij}$ represent the relative importance of criterion "i" (first column) over criterion "j" (first row), and element $a_{ji}$ is equal to $1/a_{ij}$. The diagonal values of the matrix are 1, as each criterion is equally important to itself ($a_{ii} = 1$). An example including three criteria is presented in Table 4.

Table 4. Example Comparison matrix with 3 comparison criteria and intensity of importance.

| | Resolution | Dimensional Accuracy | Surface quality |
|---|---|---|---|
| Resolution | 1 | 3 | 4 |
| Dimensional accuracy | 1/3 | 1 | 3 |
| Surface quality | 1/4 | 1/3 | 1 |

As seen in Table 4, the element $a_{12}$ is equal to $1/a_{21}$ (and same for $a_{13}$ and $a_{31}$), and the diagonal values are 1 as each comparison criterion is automatically equally important to itself.

2. Values of each column are summed. The summed values of the example in Table 4 are shown in Table 5.

Table 5. Columns of the comparison matrix summed on the last row.

| | Resolution | Dimensional Accuracy | Surface quality |
|---|---|---|---|
| Resolution | 1 | 3 | 4 |
| Dimensional accuracy | 1/3 | 1 | 3 |
| Surface quality | 1/4 | 1/3 | 1 |
| **Intensity of importance sum** | 1.583 | 4.333 | 8 |

Table 5. shows the summed intensities of importance on the last row.

3. The matrix is normalized by dividing each sell by the sum of the column where it resides. Table 6 shows the Table 4. matrix column values divided by the intensity of importance sum calculated in Table 5.

Table 6. Normalized comparison matrix

| | Resolution | Dimensional Accuracy | Surface quality |
|---|---|---|---|
| Resolution | 1/1.583 = 0.632 | 3/4.333 = 0.692 | 4/8 = 0.5 |
| Dimensional accuracy | 1/3/1.583 = 0.211 | 1/4.333 = 0.231 | 3/8 = 0.375 |
| Surface quality | 1/4/1.583 = 0.158 | 1/3/4.333 = 0.0769 | 1/8 = 0.125 |
| **SUM** | ≈1 | ≈ 1 | 1 |

As seen in Table 6, the matrix is normalized as the sum of each column now equals approximately to 1.

4. Average of each row is calculated, which gives the resulting normalized weight factors $w_i$ for each criterion on the row of the matrix. $W_i$ calculations for Table 6. normalized values are presented in Table 7.

Table 7. $W_i$ calculation as a row average for each criterion.

| | Resolution | Dimensional Accuracy | Surface quality | $w_i$ |
|---|---|---|---|---|
| Resolution | 0.632 | 0.692 | 0.5 | 0.608 |
| Dimensional accuracy | 0.211 | 0.231 | 0.375 | 0.272 |
| Surface quality | 0.158 | 0.0769 | 0.125 | 0.120 |
| **SUM** | ≈1 | ≈ 1 | 1 | 1 |

As seen in Table 7, the weight factors $w_i$ are also normalized as the sum of the weight factors equals to 1.

## 7.4 CR calculations

The logical consistency of the pairwise comparisons was verified using the Consistency Ratio, acceptable ratio being no more than 0.10. CR calculation method described by Taherdoost, (2017) proceeds through the following five steps:

1. Weighted sum vectors $d_i$ are calculated by multiplying each column of the comparison matrix by the weight factor of the comparison criterion of the column and then summing all the values of the row. The weighted sum value represents the criteria on the row

where the sum is calculated. Calculations for $d_i$ values for $w_i$ in Table 7 are shown in Table 8.

Table 8. $D_i$ calculations as a row sum for each criterion.

| | Resolution | Dimensional Accuracy | Surface quality | $d_i$ (row) |
|---|---|---|---|---|
| $w_i$ (column) | **0.608** | **0.272** | **0.120** | |
| Resolution | 0.632 x 0.608 = 0.384 | 0.692 x 0.272 = 0.188 | 0.5 x 0.120 = 0.06 | 0.632 |
| Dimensional accuracy | 0.211 x 0.608 = 0.128 | 0.231 x 0.272 = 0.0628 | 0.375 x 0.120 = 0.075 | 0.266 |
| Surface quality | 0.158 x 0.608 = 0.0961 | 0.0769 x 0.272 = 0.0209 | 0.125 x 0.120 = 0.015 | 0.132 |

2. Largest eigenvalue $\lambda_{max}$ is calculated using equation (1) as the average of all the $d_i$ / $w_i$ values.

3. A CI is calculated using the equation (2).

4. CR is calculated using the equation (3), with a RI value of 1.45 in the experimental part, according to dimension nine pairwise comparison matrix value from Table 3.

A CR of 0.10 or less are considered acceptable. If CR is more than 0.10, the comparisons should be revised until they are logically coherent.

## 7.5 Final scoring of polymer AM methods

The outcomes of the AHP process are the weight factors. After the weight factors are calculated for each prototyping scenario, they are used to calculate the final scores for each polymer AM method.

The workflow for calculating the final scores proceeds as follows:

1. Values from each row (comparison criterion) of the base score matrix is multiplied with the corresponding weight factor of the criterion calculated from the AHP workflow.

2. Values of each column (polymer AM method) are summed to calculate the final scores.

3. AM methods are then organized from the lowest to highest overall score, with the lowest score indicating the most suitable method.

# 8 Results and discussion

## 8.1 Final base score matrix

The base scores for each polymer AM method were assigned based on the qualitative summary presented in Table 1, with scoring rationale presented more accurately in chapter 7.1. The resulting base score matrix is presented in Table 9.

Table 9. Base score matrix

| comparison criteria | MEX | VPP | MJT | BJT | PBF |
|---|---|---|---|---|---|
| **smallest achievable xy resolution** | 5 | 1 | 2 | 4 | 3 |
| **dimensional accuracy** | 4 | 1 | 2 | 5 | 3 |
| **surface quality** | 5 | 1 | 1 | 4 | 3 |
| **availability of biocompatible materials** | 1 | 4 | 5 | 3 | 2 |
| **availability of biodegradable materials** | 1 | 4 | 5 | 3 | 1 |
| **mechanical strength** | 4 | 4 | 3 | 2 | 1 |
| **level of anisotropic mechanical properties** | 5 | 3 | 4 | 2 | 1 |
| **thin walled (<200 µm) structure manufacturing** | 5 | 1 | 4 | 5 | 2 |
| **post-processing requirements** | 2 | 4 | 1 | 5 | 3 |

## 8.2 Prototyping scenario 1

Question 1 determines that scenario 1 weight factors derived from the AHP method are used. As the intended use for scenario 1 prototypes are to be implanted or tested *in vivo,* question 2 eliminates any methods that do not have biocompatible or biodegradable material selections. MJT is practically eliminated, and VPP can only be used with certified biocompatible resins. Question 3 rules out methods that do not have resolution capabilities near or under 200 µm. BJT and MEX are eliminated. PBF is usable, but it should be noted that it is operating close to the resolution limit. The scenario 1 prototype is subjected to load, especially during the balloon expansion phase of implantation. The load is radially directed outwards from the centre of the tubular prototype geometry, so it is not anisotropic in nature. Question 4.1 defines that PBF is the strongest of the remaining two polymer AM methods, and VPP while usable, requires consideration in printing direction to avoid delamination. Surface quality is important for a stent-like device, but question 5.1 rules that for scenario 1, as post-processing is expected and does not affect the usability of the prototype in a negative way (in contradiction, it actually may improve the usability of the device prototype with hydrophilic or drug coating), the usability of PBF is maintained. It is noted that VPP has an advantage considering the last question with good as-manufactured surface quality. The decision-making tree eliminates the use of MJT, MEX and BJT for scenario 1.

The pairwise comparison matrix for prototyping scenario 1 is presented in Table 12 in Appendix 1. Values greater than 1 indicate that the row criterion is more important than the column criterion, and fractions indicate the opposite. The resulting weight factors $w_i$, calculated according to steps 2-5 of the AHP workflow process described in chapter 7.3, for scenario 1 are presented in Table 10. The calculation matrix for the weight factors for scenario 1 is presented in Table 13 in Appendix 1.

Table 10. Calculated weight factors for prototyping scenario 1.

| Rank | Comparison criterion | Weight factor |
|---|---|---|
| 1 | Availability of biocompatible materials | 0.30 |
| 2 | Availability of biodegradable materials | 0.23 |
| 3 | Smallest achievable xy-resolution | 0.12 |
| 4 | Thin-walled structure manufacturing | 0.12 |
| 5 | Dimensional accuracy | 0.060 |
| 6 | Mechanical strength | 0.059 |
| 7 | Level of anisotropic mechanical properties | 0.047 |
| 8 | Post-processing requirements | 0.045 |
| 9 | Surface quality | 0.028 |

CR value for scenario 1 weight factors in Table 10. is 0.089, which is lower than 0.10, making the AHP weight factors for scenario 1 logically coherent. Table 14 and Table 15 with the $d_i/w_i$ values for calculating $\lambda_{max}$ are presented in Appendix 1.

As Table 10 shows, weight factors for biocompatibility and biodegradability of the material account for 53% of the total weight factor sum, which is in line with the importance of regulatory biosafety requirements for the scenario 1 prototype material. Accuracy of the manufactured part (xy-resolution, dimensional accuracy and thin-walled structure manufacturing capability) is more important than the mechanical performance (mechanical strength and anisotropic mechanical properties). Post-processing related factors (post-processing requirements and surface quality) are the least important. This is logical for scenario 1, where post-processing is expected in any case. The final scores for prototyping scenario 1 are presented in Figure 23.

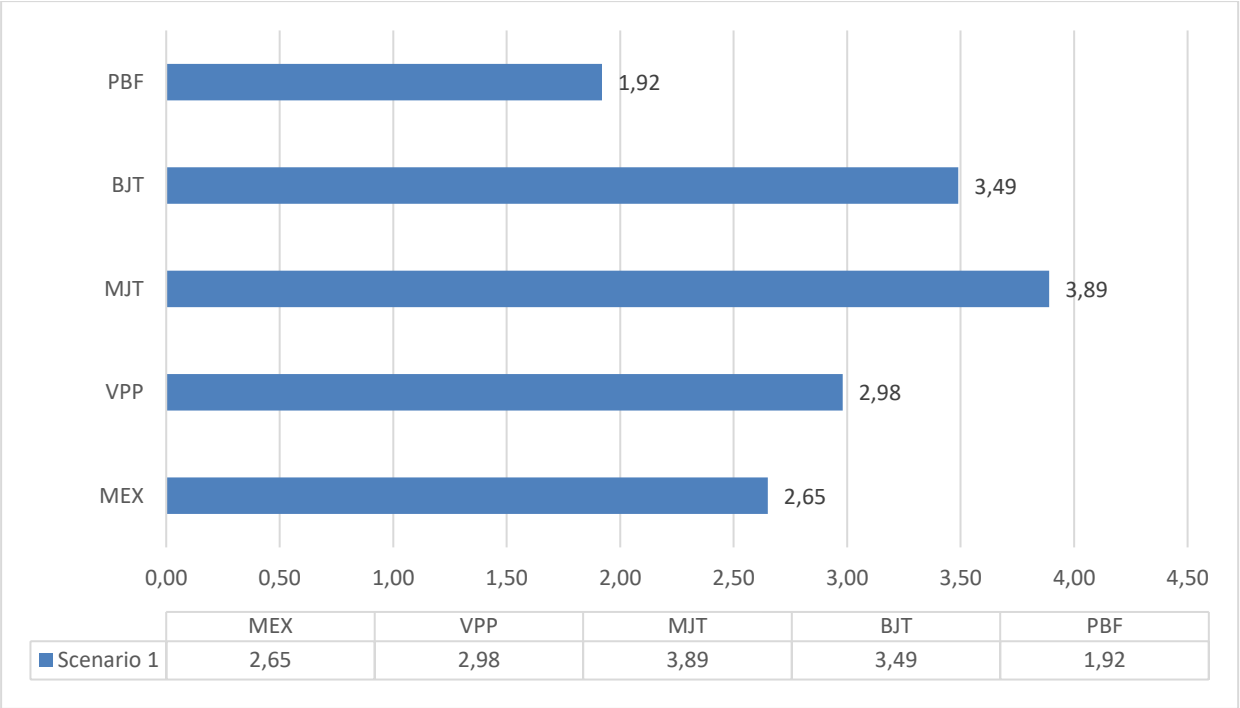


**Figure 23. Resulting scores for prototyping scenario 1.**

As Figure 23. shows, the final scores indicate that PBF is the most suitable polymer AM method for prototyping scenario 1, with the lowest score of 1.92. MEX comes second with a score of 2.65, followed by VPP with a score of 2.98. BJT places fourth with 3.49 score, and MJT comes last with the lowest score being 3.89.

It is logical that PBF should have the best score by far, as it is able to use biologically suitable materials in producing prototypes with sufficient resolution. These were set as the most important requirements in the context of *in vivo* use or implantation. Main setbacks for PBF reside in post-processing requirements, as the surface quality is very rough compared to MJT or VPP. This does not lower the score significantly with this prototyping scenario, as post-processing is expected in any case, and it also improves the mechanical properties of prototypes manufactured with PBF. While MEX can not reach the sufficient resolution, it makes sense that it ranks second highest, as seen in Figure 23, while keeping in mind that the material biocompatibility and biodegradability account to 53% of the comparison criteria weight ratio as seen in Table 10. VPP has advantages with sufficient resolution and thin-walled structure manufacturing but falls behind the top places as seen in Figure 23, due to limited biocompatible and biodegradable material selection. BJT has a better material selection, though only a little. It should be worse than VPP in scenario 1, as it is incapable of producing accurate and thin-

walled prototypes in small scales due to shrinkage associated with the manufacturing process. Even though MJT has better manufacturing accuracy and resolution, limitations in material selection place it last in scenario 1 comparison, as seen in Figure 23. The advantages of MJT, such as good as-manufactured surface quality and low post-processing requirements, do not have great importance for scenario 1.

The decision-making model produced a good result for scenario 1 when considering the regulatory restrictions for biological safety of materials. When proceeding with the logic of the decision-making tree, it is easy to see that PBF method is the most suitable, also supported by the final scores with weight factors calculated with the AHP method and presented in Figure 23. The decision-making tree ruled that only two methods, VPP and PBF, would be usable for the prototyping scenario 1. VPP is however only placed third, after MEX. It makes sense that MEX should receive a better score than VPP due to the material selection limitations of VPP, but it should be noted that MEX cannot produce prototypes in the small scales required for prototyping scenario 1. If the design would be altered in a way that the minimal resolution requirement would be closer to 300 – 600 µm, MEX would be a viable option in scenario 1 as well. On the other hand, if the requirement for biodegradation would be less important, VPP would perform better compared to PBF in producing much smaller and accurate prototypes, which can be manufactured from biocompatible materials. MJT and BJT being far behind the other methods is logical due to poor resolution and accuracy of BJT and unsuitable material selection of MJT.

## 8.3 Prototyping scenario 2

Question 1 of the decision-making tree determines the use of weight factors of scenario 2. Question 2 does not rule out any polymer AM methods, as the material selection is not critical for this type of prototyping. Even though the prototype may have detail sizes smaller than 200 µm, question 3.1 maintains the usability of MEX or BJT, which cannot reach these resolutions. The reasoning is, that the prototype can be manufactured in larger scales, such as 3:1 or 10:1, and therefore the resolution limitations are not critical. The scenario 2 prototype is not subjected to a realistic load but only has to withstand handling and minor functionality testing without failure. The mechanical strength of the manufactured parts is therefore not a limiting factor for this scenario, and question 4 indicates that all the polymer AM methods still can be used. Question 5 on the other hand differentiates some AM methods due to as-manufactured surface quality and minimal post-processing being preferable. The lower the post-processing

requirements, which also include surface quality for methods such as BJT and PBF, the better it is for rapid iteration, as the prototypes are ready for use quickly after the manufacturing process. This does not immediately eliminate methods which require post-processing, but raises the profile of MJT and MEX, which require little to no post-processing.

The AHP comparison matrix for scenario 2 is presented in Table 16 in Appendix 2. The corresponding weight factors calculated according to the AHP workflow are presented in Table 11. The weight factor calculation matrix is Table 17 in Appendix 2.

Table 11. Calculated weight factors for prototyping scenario 2.

| Rank | Comparison criterion | Weight factor |
|---|---|---|
| 1 | Post-processing requirements | 0.25 |
| 2 | Surface quality | 0.22 |
| 3 | Thin-walled structure manufacturing | 0.16 |
| 4 | Level of anisotropic mechanical properties | 0.10 |
| 5 | Dimensional accuracy | 0.086 |
| 6 | Smallest achievable xy-resolution | 0.069 |
| 7 | Mechanical strength | 0.055 |
| 8 | Availability of biocompatible materials | 0.034 |
| 9 | Availability of biodegradable materials | 0.025 |

CR value for AHP weight factors for scenario 2 presented in Table 11 is 0.07, also under 0.10, and thus logically coherent and usable for the results. Tables with the $d_i/w_i$ values for calculating $\lambda_{max}$ for scenario 2 are presented in Table 18 and Table 19 in Appendix 2.

As Table 11 shows, the weight factors for prototyping scenario 2 shifted heavily in both end points compared to prototyping scenario 1. Post-processing requirements combined with as-manufactured surface quality add to over 47% of the total weight, as can be seen in Table 11. This is in line with the rapid iteration possibility which is valuable for this kind of scenario. On the other hand, as the prototype is not intended to be used with living tissue, the material biosafety is not important, hence the low combined weight of biocompatibility and

biodegradability requirements seen in Table 11. It should be noted however, that any functional testing benefits from similar material properties for the prototyping material and the intended material for the final product. The mechanical behaviour of the manufactured prototype is closer to the final product if the material used for the prototype is close to the intended material for the final product. The final scores for prototyping scenario 2 are presented in Figure 24.

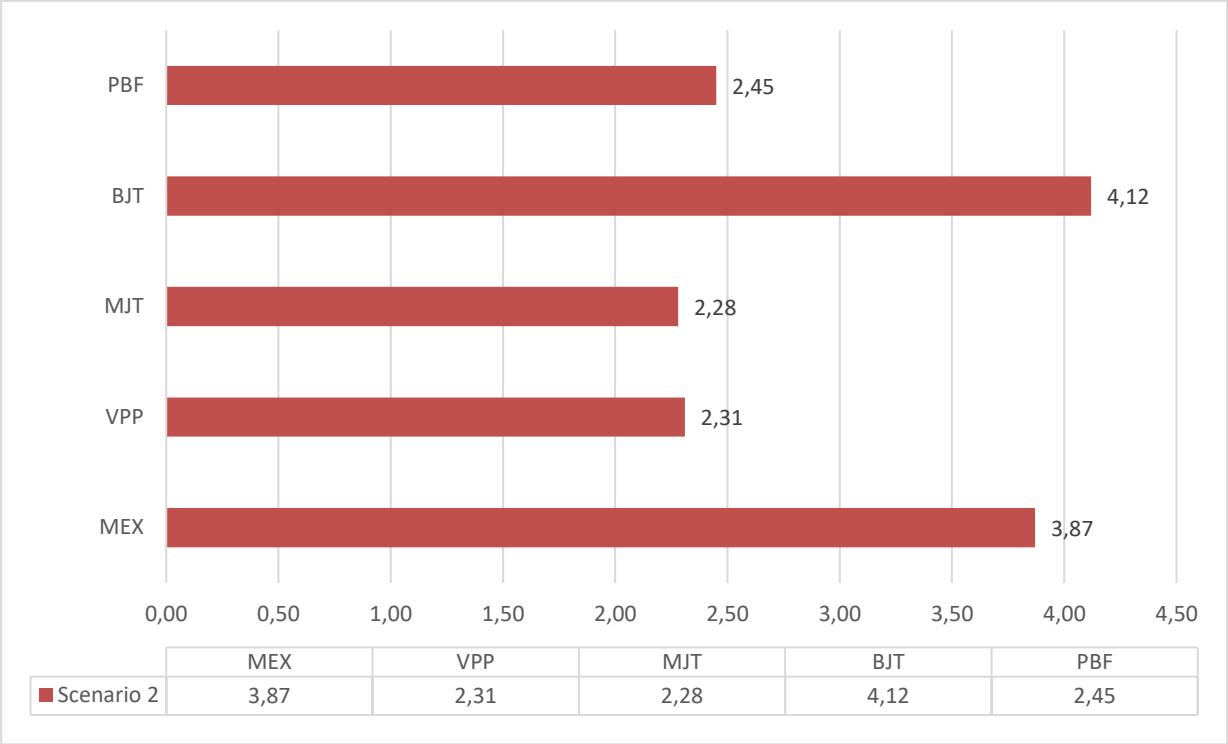


**Figure 24. Resulting scores for prototyping scenario 2.**

As seen in Figure 24, the final scores determine MJT as the best method with a score of 2.28, closely followed by VPP within roughly one percent difference at 2.31. In this scenario PBF places third with a score of 2.45. MEX if fourth with a score of 3.87, and last place is again held by BJT with 4.12 total score.

Figure 24 shows that MJT scores well and just manages to surpass VPP with the selected pairwise comparison intensities. In this case however, it should be noted that the top 3 polymer AM methods are within 0.2 score, and VPP is only 0.03 score behind MJT. Even minor changes to the pairwise comparisons may alter the top 3 positions significantly. Figure 24 shows that MEX is far behind however, due to poor as-manufactured surface quality and thin-walled structure manufacturing. The problem persist even if the scale would be somewhere between 2:1 to 5:1, but much larger scales such as 10:1 would likely make MEX a better candidate as the “thin walled” structure measurements would not be very close to the resolution limitations

or dimensional accuracy limitations of MEX. BJT places last again, as seen in Figure 24, with a score which is lower than MEX, which is not surprising due to poor surface quality, dimensional accuracy and laborious post-processing.

## 8.4 Further discussion

The decision-making tree and the AHP method for weight factor comparison and calculation gave logical outputs considering the two different scenarios. They are however prone to a subject view, for example within this thesis when they were inputs of the author only. To get a more reliable and objective viewpoint, the AHP method for comparison criteria weight factor calculation should include inputs from multiple users, and to further increase the reliability, from multiple disciplines of the device development team. It should include inputs at least from clinical experts, mechanical designers, materials experts and regulatory experts to include all relevant views of a medical device development team. The AHP method with nine comparison criteria is laborious, so automatization or tools such as python scripts or similar would speed up the process and use less time especially if multiple experts are involved in the decision-making.

Especially for scenario 2, it should be noted that even though the material choice is not restricted to biocompatible and biodegradable materials only, any kind of mechanical testing benefits from using a material which resembles the intended material as closely as possible. The model may work better if some additional or modified criteria would consider the mechanical properties of the available materials for each polymer AM method.

# 9 Conclusions

The aim of the thesis was to determine the most suitable AM method for stent-like medical device prototype fabrication, with the intended end material being a biodegradable polymer, such as PLA or PLGA. The problem was approached through literature review and a two-component decision-making model consisting of a decision-making tree and an AHP method for comparing the methods based on multiple criteria: xy-resolution, dimensional accuracy, thin-walled structure manufacturing capability, biocompatible and biodegradable material selection, mechanical strength, anisotropy of mechanical properties, surface quality and post-processing requirements. The literature review was based on AM methods and their use in biomedical applications, particularly vascular stents.

AM has gained increased interest in biomedical applications. Small medical devices with intricate geometries benefit from AM, as complex geometries are easier to manufacture, and savings can be realized through reduced logistical costs and amount of expensive waste material. Stents especially benefit from patient-specific geometries, and possibility of localized production where the stent is needed. Stent related issues like restenosis can be partly addressed by proper strut design of the stent, which is possible to realize through design flexibility enabled by AM.

Clinical application of stents fabricated with AM methods is currently limited only to urgent or low-risk cases mostly due to strict regulatory requirements set by EC or FDA. Regulatory acceptance currently favours stents manufactured with conventional manufacturing methods, such as ABSORB stent (Abbott), which is fabricated by tube extrusion and laser cutting, and has received CE marking and FDA approval.

All the polymer AM methods have distinct differences, and there is no clear winner for all potential use cases. While PBF seems to top the other methods with a combination of suitable biocompatible and biodegradable material selection and sufficient resolution capability for manufacturing stents, the as-manufactured surface quality is poor, and the parts made with PBF require substantial post-processing. VPP has the best resolution capability with some machines being able to reach sub-micrometre resolutions. The material selection for VPP is however more limited, with only some certified biocompatible resin materials and all of the materials biodegrading slowly or not at all. MEX has similar material selection to PBF, but the resolution is much worse due to nozzle size limitations and deformation during manufacturing. Post-

processing requirements are lower than for PBF, mainly consisting of removal of support structures. MJT can produce accurate parts in small scales, and with little post-processing requirements. The material selection includes only materials suitable for temporary contact with skin or mouth tissue, and not suitable for intravascular use. BJT is not optimal for small medical device manufacturing, with poor dimensional accuracy and surface quality, and high post-processing requirements.

The experimental part presented a decision-making model, which determines the most suitable AM method by combining hard-constraint filtering with the decision-making tree, and a transparent and repeatable multi-criteria decision-making method, AHP. Two different prototyping scenarios were studied: 1. Implantable / *in vivo* prototype, and 2. functional, geometry-only prototype. Scenario 1 has hard limits for biological safety of materials, and scenario 2 focuses on rapid iteration, favouring low post-processing requirements. Results for scenario 1 determined that PBF is the most suitable method, and scenario 2 had multiple close candidates: MJT, VPP and PBF in first, second, and third places respectively. Limitations of the decision-making framework and proposals for further development are discussed in Chapter 8.4.

## References

Ahn, J.-H., Kim, J., Han, G., Kim, D., Cheon, K.-H., Lee, H., Kim, H.-E., Kim, Y.-J., Jang, T.-S., & Jung, H.-D. (2021). 3D-printed biodegradable composite scaffolds with significantly enhanced mechanical properties via the combination of binder jetting and capillary rise infiltration process. *Additive Manufacturing*, *41*, 101988. https://doi.org/10.1016/j.addma.2021.101988

Ali, F., Kalva, S. N., & Koc, M. (2024). Advancements in 3D printing techniques for biomedical applications: A comprehensive review of materials consideration, post processing, applications, and challenges. *Discover Materials*, *4*(1), 53. https://doi.org/10.1007/s43939-024-00115-4

Benyathiar, P., Selke, S. E., Harte, B. R., & Mishra, D. K. (2021). The Effect of Irradiation Sterilization on Poly(Lactic) Acid Films. *Journal of Polymers and the Environment*, *29*(2), 460–471. https://doi.org/10.1007/s10924-020-01892-8

Bianchi, I., Forcellese, A., Mancia, T., Simoncini, M., & Vita, A. (2022). Process parameters effect on environmental sustainability of composites FFF technology. *Materials and Manufacturing Processes*, *37*(5), 591–601. https://doi.org/10.1080/10426914.2022.2049300

Bikas, H., Stavropoulos, P., & Chryssolouris, G. (2016). Additive manufacturing methods and modelling approaches: A critical review. *The International Journal of Advanced Manufacturing Technology*, *83*(1), 389–405. https://doi.org/10.1007/s00170-015-7576-2

*Biocompatible Materials | Stratasys Support Center*. (n.d.). Stratasys. Retrieved April 21, 2026, from https://support.stratasys.com/en/Materials/PolyJet/Biocompatible

Bosch, A., Ausellé-Bosch, S., Ponce, C., Rubio, C., Puig, T., Ciurana, J., & Guerra, A. J. (2025). Analysis of printing and post-curing parameters to enhance physicochemical and biomechanical properties of polymeric stents produced by tubular vat photopolymerization. *Progress in Additive Manufacturing*, *10*(9), 5993–6006. https://doi.org/10.1007/s40964-025-00948-2

Bouzaglou, O., Golan, O., & Lachman, N. (2023). Process Design and Parameters Interaction in Material Extrusion 3D Printing: A Review. *Polymers*, *15*(10). https://doi.org/10.3390/polym15102280

Braghirolli, D. I., Fin, M. D. C., Steffens, D., Gamba, D., Pranke, P. H. L., & Petzhold, C. L. (2011). *The effect of sterilization on the degradation of PLGA nanofibers for use in tissue engineering*. https://lume.ufrgs.br/handle/10183/285056

Burt, H. M., & Hunter, W. L. (2006). Drug-eluting stents: An innovative multidisciplinary drug delivery platform. *Advanced Drug Delivery Reviews, Drug-Eluting Stents: An Innovative Multidisciplinary Drug Delivery Platform*, *58*(3), 345–346. https://doi.org/10.1016/j.addr.2006.02.001

Chartrain, N. A., Williams, C. B., & Whittington, A. R. (2018). A review on fabricating tissue scaffolds using vat photopolymerization. *Acta Biomaterialia*, *74*, 90–111. https://doi.org/10.1016/j.actbio.2018.05.010

Corrado, F., Di Maio, L., Palmero, P., Coppola, B., Abbas, Z., La Gatta, A., Schiraldi, C., & Scarfato, P. (2025). Vat photo-polymerization 3D printing of gradient scaffolds for osteochondral tissue regeneration. *Acta Biomaterialia*, *200*, 67–86. https://doi.org/10.1016/j.actbio.2025.05.042

Costa, J. R., Chamie, D., Sousa, J. E., & Abizaid, A. (2018). *Stents* and the Endothelium. In P. L. Da Luz, P. Libby, A. C. P. Chagas, & F. R. M. Laurindo (Eds.), *Endothelium and Cardiovascular Diseases* (pp. 597–608). Academic Press. https://doi.org/10.1016/B978-0-12-812348-5.00041-6

Dobrzańska-Danikiewicz, A. D., & Bączyk, A. (2024). A review of additive manufacturing technologies. *Archives of Materials Science and Engineering*, *128*(2), 68–85. Scopus. https://doi.org/10.5604/01.3001.0054.8755

Farazin, A., Darghiasi, S. F., & Gheisizadeh, A. (2025). Transforming Medical Manufacturing: Groundbreaking Innovations Redefining Healthcare. *Journal of Computational Applied Mechanics*, *56*(1), 1–14. Scopus. https://doi.org/10.22059/jcamech.2024.384068.1266

Flege, C., Vogt, F., Höges, S., Jauer, L., Borinski, M., Schulte, V. A., Hoffmann, R., Poprawe, R., Meiners, W., Jobmann, M., Wissenbach, K., & Blindt, R. (2013). Development and

characterization of a coronary polylactic acid stent prototype generated by selective laser melting. *Journal of Materials Science: Materials in Medicine*, *24*(1), 241–255. https://doi.org/10.1007/s10856-012-4779-z

Ford, S., Despeisse, M., & Viljakainen, A. (2015, November 2). *Extending product life through additive manufacturing: The sustainability implications*.

Fratini, C., Zhang, Y., Moroni, S., Tiboni, M., Ong, H. X., Young, P. M., Casettari, L., & Traini, D. (2025). Combining innovation and sustainable development in the 3D printing manufacturing of drug delivery and testing devices. *International Journal of Pharmaceutics*, *679*, 125751. https://doi.org/10.1016/j.ijpharm.2025.125751

Goel, S., Raj, S., Sharma, A., Gidwani, U., Frankel, R., & Shani, J. (2017). Bioresorbable Coronary Scaffolds: Current State of Evidence. *EMJ Cardiol Cardiology 5.1 2017*, *5*(1), 53–61. https://doi.org/10.33590/emjcardiol/10311110

Gonçalves, A. M., Moreira, A., Weber, A., Williams, G. R., & Costa, P. F. (2021). Osteochondral Tissue Engineering: The Potential of Electrospinning and Additive Manufacturing. *Pharmaceutics*, *13*(7). https://doi.org/10.3390/pharmaceutics13070983

Guerra, A., Roca, A., & de Ciurana, J. (2017). A novel 3D additive manufacturing machine to biodegradable stents. *Procedia Manufacturing, Manufacturing Engineering Society International Conference 2017, MESIC 2017, 28-30 June 2017, Vigo (Pontevedra), Spain*, *13*, 718–723. https://doi.org/10.1016/j.promfg.2017.09.118

Gülcan, O., Günaydın, K., & Tamer, A. (2021). The State of the Art of Material Jetting—A Critical Review. *Polymers*, *13*(16), Article 16. https://doi.org/10.3390/polym13162829

Hong, J., Bae, I.-S., Kang, H. I., Kim, J. H., & Jwa, C. (2023). Development of a Pedicle Screw Fixation Simulation Model for Surgical Training Using a 3-Dimensional Printer. *World Neurosurgery*, *171*, e554–e559. https://doi.org/10.1016/j.wneu.2022.12.065

Hsiao, H.-M., Lin, C.-H., Liao, Y.-C., Chen, H.-Y., & Wang, T.-W. (2014). Hemodynamic behavior of coronary stents in straight and curved arteries. *Current Nanoscience*, *10*(2), 205–211. Scopus. https://doi.org/10.2174/15734137096661311290000833

Iqbal, J., Gunn, J., & Serruys, P. W. (2013). Coronary stents: Historical development, current status and future directions. *British Medical Bulletin*, *106*(1), 193–211. https://doi.org/10.1093/bmb/ldt009

*ISO 10993-1:2018*. (n.d.). ISO. Retrieved August 11, 2025, from https://www.iso.org/standard/68936.html

*ISO/ASTM 52900:2021(en), Additive manufacturing—General principles—Fundamentals and vocabulary*. (n.d.). Retrieved April 7, 2025, from https://www.iso.org/obp/ui#iso:std:iso-astm:52900:ed-2:v1:en

Kállai, Z., Kipping, J., Bremer, J., & Schüppstuhl, T. (2025). A Preliminary study: Support-free manufacturing of rotationally symmetric pipes from continuous carbon fiber reinforced polymers with multi-axis 3D printing. *Mater. Res. Proc.*, *54*, 344–353. https://doi.org/10.21741/9781644903599-38

Khalaj, R., Tabriz, A. G., Okereke, M. I., & Douroumis, D. (2021). 3D printing advances in the development of stents. *International Journal of Pharmaceutics*, *609*, 121153. https://doi.org/10.1016/j.ijpharm.2021.121153

Kiousis, D. E., Wulff, A. R., & Holzapfel, G. A. (2009). Experimental studies and numerical analysis of the inflation and interaction of vascular balloon catheter-stent systems. *Annals of Biomedical Engineering*, *37*(2), 315–330. https://doi.org/10.1007/s10439-008-9606-9

Kladovasilakis, N., Kyriakidis, I. F., Tzimtzimis, E. K., Pechlivani, E. M., Tsongas, K., & Tzetzis, D. (2025). Development of 4D-Printed Arterial Stents Utilizing Bioinspired Architected Auxetic Materials. *Biomimetics*, *10*(2). Scopus. https://doi.org/10.3390/biomimetics10020078

Kronenberger, R., Kazma, R., Amirabadi, A., Uribe, L. V., Talevi, G., Kaya, G. E., Brande, N. V. den, Abadi, R. H., Kalteremidou, K.-A., Hemelrijck, D. V., Baert, K., Hauffman, T., Soete, J., Pannone, L., Paparella, A. M., Eltsov, I., Chierchia, G. B., Meir, M. L., Gharaviri, A., & Asmundis, C. de. (2025). Impact of Disinfection and Sterilization on 3D-Printing Resin Performance for Surgical Guides in Cardiac Ablation Surgery. *Bioengineering*, *12*(9). https://doi.org/10.3390/bioengineering12090924

Krug, N., Zarges, J.-C., & Heim, H.-P. (2024). Influence of ethylene oxide and gamma irradiation sterilization processes on the degradation behaviour of poly(lactic acid) (PLA) in the course of artificially accelerated aging. *Polymer Testing*, *132*, 108362. https://doi.org/10.1016/j.polymertesting.2024.108362

Kulker, D., Pepin, J., Rosa, B., Laure, B., Venin, M., Biglione, J., & Pare, A. (2025). Physico-mechanical characterization of 3D-printed PLGA for patient-specific resorbable implants in craniofacial surgery. *Scientific Reports*, *15*(1), 22225. https://doi.org/10.1038/s41598-025-07617-y

Liu, S.-F., Hou, Z.-W., Lin, L., Li, Z., & Sun, H.-B. (2023). 3D Laser Nanoprinting of Functional Materials. *Advanced Functional Materials*, *33*(39), 2211280. https://doi.org/10.1002/adfm.202211280

Magri, A. E., Bencaid, S. E., Vanaei, H. R., & Vaudreuil, S. (2022). Effects of Laser Power and Hatch Orientation on Final Properties of PA12 Parts Produced by Selective Laser Sintering. *Polymers*, *14*(17). https://doi.org/10.3390/polym14173674

Mançanares, C. G., de S. Zancul, E., Cavalcante da Silva, J., & Cauchick Miguel, P. A. (2015). Additive manufacturing process selection based on parts' selection criteria. *The International Journal of Advanced Manufacturing Technology*, *80*(5), 1007–1014. https://doi.org/10.1007/s00170-015-7092-4

Modi, K., Soos, M. P., & Mahajan, K. (2025). Stent Thrombosis. In *StatPearls*. StatPearls Publishing. http://www.ncbi.nlm.nih.gov/books/NBK441908/

Moore, S. S., O'Sullivan, K. J., & Verdecchia, F. (2016). Shrinking the Supply Chain for Implantable Coronary Stent Devices. *Annals of Biomedical Engineering*, *44*(2), 497–507. https://doi.org/10.1007/s10439-015-1471-8

Nguyen, A. K., & Narayan, R. J. (2017). Two-photon polymerization for biological applications. *Materials Today*, *20*(6), 314–322. https://doi.org/10.1016/j.mattod.2017.06.004

Omeh, D. J., & Shlofmitz, E. (2025). Restenosis of Stented Coronary Arteries. In *StatPearls*. StatPearls Publishing. http://www.ncbi.nlm.nih.gov/books/NBK545139/

Park, S. A., Lee, S. J., Lim, K. S., Bae, I. H., Lee, J. H., Kim, W. D., Jeong, M. H., & Park, J.-K. (2015). *In vivo* evaluation and characterization of a bio-absorbable drug-coated stent fabricated using a 3D-printing system. *Materials Letters*, *141*, 355–358. https://doi.org/10.1016/j.matlet.2014.11.119

Pattison, T. G., Wang, S., Miller, R. D., Liu, G., & Qiao, G. G. (2022). 3D nanoprinting via spatially controlled assembly and polymerization. *Nature Communications*, *13*(1), 1941. https://doi.org/10.1038/s41467-022-29432-z

Piedra-Cascón, W., Pérez-López, J., Veiga-López, B., Oteo-Morilla, C., Pose-Rodriguez, J. M., & Gallas-Torreira, M. (2024). Influence of base designs on the manufacturing accuracy of vat-polymerized diagnostic casts using two different technologies. *The Journal of Prosthetic Dentistry*, *132*(2), 453.e1-453.e9. https://doi.org/10.1016/j.prosdent.2024.04.009

Rebelo, R., Fernandes, M., & Fangueiro, R. (2017). Biopolymers in Medical Implants: A Brief Review. *Procedia Engineering, 3rd International Conference on Natural Fibers: Advanced Materials for a Greener World, ICNF 2017, 21-23 June 2017, Braga, Portugal*, *200*, 236–243. https://doi.org/10.1016/j.proeng.2017.07.034

Roberson, D. A., Espalin ,D., & and Wicker, R. B. (2013). 3D printer selection: A decision-making evaluation and ranking model. *Virtual and Physical Prototyping*, *8*(3), 201–212. https://doi.org/10.1080/17452759.2013.830939

S., A. D., P., S. P. A., Naveen, J., Khan, T., & Khahro, S. H. (2024). Advancement in biomedical implant materials—A mini review. *Frontiers in Bioengineering and Biotechnology*, *12*. https://doi.org/10.3389/fbioe.2024.1400918

Saaty, T. (2008). Decision making with the Analytic Hierarchy Process. *Int. J. Services Sciences Int. J. Services Sciences*, *1*, 83–98. https://doi.org/10.1504/IJSSCI.2008.017590

Shakibania, S., Khakbiz, M., Kilic Bektas, C., Ghazanfari, L., Tavakoli Banizi, M., & Lee, K.-B. (2022). *A review of 3D printing technology for rapid medical diagnostic tools*. https://doi.org/10.1039/D1ME00178G

Singh, T., Jain, V., Kumar, H., & Nagdeve, L. (2025). Parametric analysis of wear and surface roughness of additive manufactured ABS parts from indigenous ABS filament. *Engineering Research Express*, *7*(4), 045518. https://doi.org/10.1088/2631-8695/ae0b34

Spina, R. (2025). Surface appearance of poly lactic acid due to variations in material extrusion processing parameters. *Scientific Reports*, *15*(1), 29788. https://doi.org/10.1038/s41598-025-14484-0

Taherdoost, H. (2017). Decision Making Using the Analytic Hierarchy Process (AHP); A Step by Step Approach. *International Journal of Economics and Management Systems*, *02*. https://www.iaras.org/home/caijems/decision-making-using-the-analytic-hierarchy-process-ahp-a-step-by-step-approach

*Technical Considerations for Additive Manufactured Medical Devices—Guidance for Industry and Food and Drug Administration Staff*. (n.d.).

Tsui, P.-T., & Lau, C. -l. (2007). Severe plaque prolapse after stenting a lesion with large areas of necrotic core. *Heart*, *93*(11), 1350–1350. https://doi.org/10.1136/hrt.2006.104190

Umemoto, T., de Donato, G., Pacchioni, A., Reimers, B., Ferrante, G., Isobe, M., & Setacci, C. (2017). Optical coherence tomography assessment of newgeneration mesh-covered stents after carotid stenting. *EuroIntervention: Journal of EuroPCR in Collaboration with the Working Group on Interventional Cardiology of the European Society of Cardiology*, *13*(11), 1347–1354. https://doi.org/10.4244/EIJ-D-16-00866

Vakiti, T., Suranani, S., & Kuppusamy, R. R. P. (2025). Effect of print orientations, layer thicknesses, and weathering on the mechanical properties, failure mechanism, and service life of 3D-printed photocured resin parts. *Polymer Engineering & Science*, *65*(2), 797–815. https://doi.org/10.1002/pen.27043

van Lith, R., Baker, E., Ware, H., Yang, J., Farsheed, A. C., Sun, C., & Ameer, G. (2016). 3D-Printing Strong High-Resolution Antioxidant Bioresorbable Vascular Stents. *Advanced Materials Technologies*, *1*(9). Scopus. https://doi.org/10.1002/admt.201600138

Wang, Z., & Yang, Y. (2021). Application of 3D Printing in Implantable Medical Devices. *BioMed Research International*, *2021*. https://doi.org/10.1155/2021/6653967

Yue Ma et al., C.-J. S. (2024). Advances in 4D printing of biodegradable photopolymers. *ResearchGate*. https://doi.org/10.1002/rpm.20240008

Zhou, L., Miller, J., Vezza, J., Mayster, M., Raffay, M., Justice, Q., Tamimi, Z. A., Hansotte, G., Sunkara, L. D., & Bernat, J. (2024). Additive Manufacturing: A Comprehensive Review. *Sensors*, *24*(9). https://doi.org/10.3390/s24092668

Zhu, Y., Guo, S., Ravichandran, D., Ramanathan, A., Sobczak, M. T., Sacco, A. F., Patil, D., Thummalapalli, S. V., Pulido, T. V., Lancaster, J. N., Yi, J., Cornella, J. L., Lott, D. G., Chen, X., Mei, X., Zhang, Y. S., Wang, L., Wang, X., Zhao, Y., … Song, K. (2025). 3D-Printed Polymeric Biomaterials for Health Applications. *Advanced Healthcare Materials*, *14*(1). Scopus. https://doi.org/10.1002/adhm.202402571

# Appendices

## Appendix 1 Matrices and calculations for scenario 1

AHP comparison matrix for scenario 1 are presented in Table 12, with last row having sums of each column for the normalization of the matrix.

Table 12. Pairwise comparison matrix of scenario 1.

| | Res. | Dim. | Surf. | Biocomp. | Biodegr. | Mech. | Aniso. | Thin-w. | Post-p. |
|---|---|---|---|---|---|---|---|---|---|
| Resolution | 1,000 | 3,000 | 4,000 | 0,167 | 0,200 | 3,000 | 3,000 | 2,000 | 4,000 |
| Dim. Accuracy | 0,333 | 1,000 | 3,000 | 0,167 | 0,200 | 0,500 | 2,000 | 0,333 | 3,000 |
| Surf. quality | 0,250 | 0,333 | 1,000 | 0,143 | 0,167 | 0,333 | 0,500 | 0,250 | 1,000 |
| Biocomp. | 6,000 | 6,000 | 7,000 | 1,000 | 2,000 | 5,000 | 4,000 | 3,000 | 6,000 |
| Biodegr. | 5,000 | 5,000 | 6,000 | 0,500 | 1,000 | 4,000 | 4,000 | 3,000 | 5,000 |
| mech. Strength | 0,333 | 2,000 | 3,000 | 0,200 | 0,250 | 1,000 | 2,000 | 0,333 | 0,333 |
| Anisotropy | 0,333 | 0,500 | 2,000 | 0,250 | 0,250 | 0,500 | 1,000 | 0,250 | 2,000 |
| Thin-wall | 0,500 | 3,000 | 4,000 | 0,333 | 0,333 | 3,000 | 4,000 | 1,000 | 3,000 |
| Post-proc. | 0,250 | 0,333 | 1,000 | 0,167 | 0,200 | 3,000 | 0,500 | 0,333 | 1,000 |
| **SUM** | **14,000** | **21,167** | **31,000** | **2,926** | **4,600** | **20,333** | **21,000** | **10,500** | **25,333** |

The normalized matrix, where each cell has been divided by the sum of the column (last row in Table 12) for scenario 1 is presented in Table 13, with the last column showing the weight factors of each row criterion. The weight factor ($w_i$) is the average of each row values of the normalized matrix.

Table 13. Normalized matrix of scenario 1.

| | Res. | Dim. | Surf. | Biocomp. | Biodegr. | Mech. | Aniso. | Thin-w. | Post-p. | $\mathbf{w_i}$ |
|---|---|---|---|---|---|---|---|---|---|---|
| Resolution | 0,071 | 0,142 | 0,129 | 0,057 | 0,043 | 0,148 | 0,143 | 0,190 | 0,158 | **0,120** |
| Dim. Accuracy | 0,024 | 0,047 | 0,097 | 0,057 | 0,043 | 0,025 | 0,095 | 0,032 | 0,118 | **0,060** |
| Surf. quality | 0,018 | 0,016 | 0,032 | 0,049 | 0,036 | 0,016 | 0,024 | 0,024 | 0,039 | **0,028** |
| Biocomp. | 0,429 | 0,283 | 0,226 | 0,342 | 0,435 | 0,246 | 0,190 | 0,286 | 0,237 | **0,297** |
| Biodegr. | 0,357 | 0,236 | 0,194 | 0,171 | 0,217 | 0,197 | 0,190 | 0,286 | 0,197 | **0,227** |
| mech. Strength | 0,024 | 0,094 | 0,097 | 0,068 | 0,054 | 0,049 | 0,095 | 0,032 | 0,013 | **0,059** |
| Anisotropy | 0,024 | 0,024 | 0,065 | 0,085 | 0,054 | 0,025 | 0,048 | 0,024 | 0,079 | **0,047** |
| Thin-wall | 0,036 | 0,142 | 0,129 | 0,114 | 0,072 | 0,148 | 0,190 | 0,095 | 0,118 | **0,116** |
| Post-proc. | 0,018 | 0,016 | 0,032 | 0,057 | 0,043 | 0,148 | 0,024 | 0,032 | 0,039 | **0,045** |

Weighted sum vectors ($d_i$) of scenario 1 are presented in Table 14, calculated by multiplying each column (of pairwise comparison matrix) with the calculated weight factors and summing the rows to the final column.

Table 14. Weight sum vector calculation matrix for prototyping scenario 1.

| | Res. | Dim. Acc. | Surf. | Bioc. | Biod. | Mech. | Aniso. | Thin-w | Post-p. | $d_i$ |
|---|---|---|---|---|---|---|---|---|---|---|
| **$w_i$** | **0,120** | **0,060** | **0,028** | **0,297** | **0,227** | **0,059** | **0,047** | **0,116** | **0,045** | |
| Resolution | 0,120 | 0,179 | 0,113 | 0,050 | 0,045 | 0,176 | 0,142 | 0,232 | 0,182 | **1,239** |
| Dim. Accuracy | 0,040 | 0,060 | 0,085 | 0,050 | 0,045 | 0,029 | 0,095 | 0,039 | 0,136 | **0,579** |
| Surf. quality | 0,030 | 0,020 | 0,028 | 0,042 | 0,038 | 0,020 | 0,024 | 0,029 | 0,045 | **0,276** |
| Biocomp. | 0,721 | 0,359 | 0,198 | 0,297 | 0,455 | 0,293 | 0,190 | 0,348 | 0,273 | **3,132** |
| Biodegr. | 0,601 | 0,299 | 0,170 | 0,149 | 0,227 | 0,234 | 0,190 | 0,348 | 0,227 | **2,444** |
| mech. Strength | 0,040 | 0,120 | 0,085 | 0,059 | 0,057 | 0,059 | 0,095 | 0,039 | 0,015 | **0,568** |
| Anisotropy | 0,040 | 0,030 | 0,057 | 0,074 | 0,057 | 0,029 | 0,047 | 0,029 | 0,091 | **0,454** |
| Thin-wall | 0,060 | 0,179 | 0,113 | 0,099 | 0,076 | 0,176 | 0,190 | 0,116 | 0,136 | **1,145** |
| Post-proc. | 0,030 | 0,020 | 0,028 | 0,050 | 0,045 | 0,176 | 0,024 | 0,039 | 0,045 | **0,457** |

The $\lambda_{max}$ values for scenario 1 are presented in Table 15. The $\lambda_{max}$ is the average of each $d_i$ divided by $w_i$.

Table 15. $\lambda_{max}$ values for prototyping scenario 1.

| | $d_i$ / $w_i$ |
|---|---|
| Resolution | 10,315 |
| Dim. Accuracy | 9,676 |
| Surf. quality | 9,772 |
| Biocomp. | 10,546 |
| Biodegr. | 10,756 |
| mech. Strength | 9,697 |
| Anisotropy | 9,579 |
| Thin-wall | 9,866 |
| Post-proc. | 10,053 |
| $\lambda_{max}$ (average) | **10,029** |

## Appendix 2 Matrices and calculations for scenario 2

The pairwise comparison matrix for prototyping scenario 2 is presented in Table 16.

Table 16. Pairwise comparison matrix of scenario 2.

| | Res. | Dim. | Surf. | Biocomp. | Biodegr. | Mech. | Aniso. | Thin-w. | Post-p. |
|---|---|---|---|---|---|---|---|---|---|
| Resolution | 1,00 | 0,33 | 0,20 | 5,00 | 5,00 | 1,00 | 0,33 | 0,33 | 0,25 |
| Dim. Accuracy | 3,00 | 1,00 | 0,20 | 3,00 | 4,00 | 3,00 | 0,50 | 0,25 | 0,25 |
| Surf. quality | 5,00 | 5,00 | 1,00 | 5,00 | 6,00 | 3,00 | 2,00 | 2,00 | 1,00 |
| Biocomp. | 0,20 | 0,33 | 0,20 | 1,00 | 2,00 | 0,50 | 0,25 | 0,25 | 0,20 |
| Biodegr. | 0,20 | 0,25 | 0,17 | 0,50 | 1,00 | 0,33 | 0,25 | 0,20 | 0,17 |
| mech. Strength | 1,00 | 0,33 | 0,33 | 2,00 | 3,00 | 1,00 | 0,50 | 0,33 | 0,20 |
| Anisotropy | 3,00 | 2,00 | 0,50 | 4,00 | 4,00 | 2,00 | 1,00 | 0,33 | 0,25 |
| Thin-wall | 3,00 | 4,00 | 0,50 | 4,00 | 5,00 | 3,00 | 3,00 | 1,00 | 0,33 |
| Post-proc. | 4,00 | 4,00 | 1,00 | 5,00 | 6,00 | 5,00 | 4,00 | 3,00 | 1,00 |
| SUM | **20,40** | **17,25** | **4,10** | **29,50** | **36,00** | **18,83** | **11,83** | **7,70** | **3,65** |

Normalized matrix of scenario 2 is presented in Table 11, with $w_i$ values calculated on the last column.

Table 17. Normalized matrix of scenario 2.

| | Res. | Dim. | Surf. | Biocomp. | Biodegr. | Mech. | Aniso. | Thin-w. | Post-p. | $w_i$ |
|---|---|---|---|---|---|---|---|---|---|---|
| Resolution | 0,049 | 0,019 | 0,049 | 0,169 | 0,139 | 0,053 | 0,028 | 0,043 | 0,068 | 0,069 |
| Dim. Accuracy | 0,147 | 0,058 | 0,049 | 0,102 | 0,111 | 0,159 | 0,042 | 0,032 | 0,068 | 0,085 |
| Surf. quality | 0,245 | 0,290 | 0,244 | 0,169 | 0,167 | 0,159 | 0,169 | 0,260 | 0,274 | 0,220 |
| Biocomp. | 0,010 | 0,019 | 0,049 | 0,034 | 0,056 | 0,027 | 0,021 | 0,032 | 0,055 | 0,034 |
| Biodegr. | 0,010 | 0,014 | 0,041 | 0,017 | 0,028 | 0,018 | 0,021 | 0,026 | 0,046 | 0,024 |
| mech. Strength | 0,049 | 0,019 | 0,081 | 0,068 | 0,083 | 0,053 | 0,042 | 0,043 | 0,055 | 0,055 |
| Anisotropy | 0,147 | 0,116 | 0,122 | 0,136 | 0,111 | 0,106 | 0,085 | 0,043 | 0,068 | 0,104 |
| Thin-wall | 0,147 | 0,232 | 0,122 | 0,136 | 0,139 | 0,159 | 0,254 | 0,130 | 0,091 | 0,157 |
| Post-proc. | 0,196 | 0,232 | 0,244 | 0,169 | 0,167 | 0,265 | 0,338 | 0,390 | 0,274 | 0,253 |

Weighted sum vectors ($d_i$) of scenario 2 are presented in Table 18.

Table 18. Weight sum vector calculation matrix for prototyping scenario 2.

| | Res. | Dim. | Surf. | Biocomp. | Biodegr. | Mech. | Aniso. | Thin-w. | Post-p. | $d_i$ |
|---|---|---|---|---|---|---|---|---|---|---|
| $w_i$ | 0,07 | 0,09 | 0,22 | 0,03 | 0,02 | 0,05 | 0,10 | 0,16 | 0,25 | |
| Resolution | 0,07 | 0,03 | 0,04 | 0,17 | 0,12 | 0,05 | 0,03 | 0,05 | 0,06 | **0,64** |
| Dim. Accuracy | 0,21 | 0,09 | 0,04 | 0,10 | 0,10 | 0,16 | 0,05 | 0,04 | 0,06 | **0,85** |
| Surf. quality | 0,34 | 0,43 | 0,22 | 0,17 | 0,15 | 0,16 | 0,21 | 0,31 | 0,25 | **2,24** |
| Biocomp. | 0,01 | 0,03 | 0,04 | 0,03 | 0,05 | 0,03 | 0,03 | 0,04 | 0,05 | **0,31** |
| Biodegr. | 0,01 | 0,02 | 0,04 | 0,02 | 0,02 | 0,02 | 0,03 | 0,03 | 0,04 | **0,23** |
| mech. Strength | 0,07 | 0,03 | 0,07 | 0,07 | 0,07 | 0,05 | 0,05 | 0,05 | 0,05 | **0,52** |
| Anisotropy | 0,21 | 0,17 | 0,11 | 0,13 | 0,10 | 0,11 | 0,10 | 0,05 | 0,06 | **1,05** |
| Thin-wall | 0,21 | 0,34 | 0,11 | 0,13 | 0,12 | 0,16 | 0,31 | 0,16 | 0,08 | **1,63** |
| Post-proc. | 0,27 | 0,34 | 0,22 | 0,17 | 0,15 | 0,27 | 0,42 | 0,47 | 0,25 | **2,56** |

The $\lambda_{max}$ values for scenario 2 are presented in Table 19. The $\lambda_{max}$ is the average of each $d_i$ divided by $w_i$.

Table 19. $\lambda_{max}$ values for prototyping scenario 2.

| | $d_i/w_i$ |
|---|---|
| Resolution | 9,258171 |
| Dim. Accuracy | 9,983399 |
| Surf. quality | 10,21355 |
| Biocomp. | 9,28243 |
| Biodegr. | 9,431069 |
| mech. Strength | 9,479876 |
| Anisotropy | 10,09836 |
| Thin-wall | 10,41828 |
| Post-proc. | 10,14053 |
| $\lambda_{max}$ | **9,811742** |